

Research Paper

Interstitial Fluid Shear Stress Induces the Synthetic Phenotype Switching of VSMCs to Release Pro-calcified Extracellular Vesicles via EGFR-MAPK-KLF5 Pathway

Wenbo Gao^{1*}, Kaiyun Gu^{2*}, Lunjie Ma¹, Fan Yang¹, Li Deng¹, Yaojia Zhang¹, Michael Z. Miao³, Wenjun Li³, Gang Li⁴, Hong Qian⁵, Zhen Zhang⁶, Guixue Wang^{7,8}, Hongchi Yu¹, Xiaoheng Liu¹

1. Institute of Biomedical Engineering, West China School of Basic Medical Sciences & Forensic Medicine, Sichuan University, Chengdu 610041, China.
2. Department of Cardiac Surgery, Children's Hospital, Zhejiang University School of Medicine, National Clinical Research Center for Child Health, Hangzhou 310052, China.
3. Division of Oral & Craniofacial Health Sciences, Adams School of Dentistry, University of North Carolina at Chapel Hill, NC, 27599, USA.
4. Department of Genome Sciences, University of Washington, William H. Foege Hall, 3720 15th Ave NE, Seattle 98195, USA.
5. Department of Cardiovascular Surgery, West China Hospital of Sichuan University, Chengdu 610041, China.
6. Department of Cardiology, The Third People's Hospital of Chengdu, Affiliated Hospital of Southwest Jiaotong University, Chengdu 610031, China.
7. Key Laboratory for Biorheological Science and Technology of Ministry of Education, State and Local Joint Engineering Laboratory for Vascular Implants, Bioengineering College of Chongqing University, Chongqing 400030, China.
8. JinFeng Laboratory, Chongqing 401329, China.

*These authors contribute equally to this work.

 Corresponding authors: Hongchi Yu: yuhongchi@scu.edu.cn; Xiaoheng Liu: liuxiaohg@scu.edu.cn.

© The author(s). This is an open access article distributed under the terms of the Creative Commons Attribution License (<https://creativecommons.org/licenses/by/4.0/>). See <http://ivyspring.com/terms> for full terms and conditions.

Received: 2023.10.03; Accepted: 2024.04.20; Published: 2024.04.29

Abstract

Phenotypic switching (from contractile to synthetic) of vascular smooth muscle cells (VSMCs) is essential in the progression of atherosclerosis. The damaged endothelium in the atherosclerotic artery exposes VSMCs to increased interstitial fluid shear stress (IFSS). However, the precise mechanisms by which increased IFSS influences VSMCs phenotypic switching are unrevealed. Here, we employed advanced numerical simulations to calculate IFSS values accurately based on parameters acquired from patient samples. We then carefully investigated the phenotypic switching and extracellular vesicles (EVs) secretion of VSMCs under various IFSS conditions. By employing a comprehensive set of approaches, we found that VSMCs exhibited synthetic phenotype upon atherosclerotic IFSS. This synthetic phenotype is the upstream regulator for the enhanced secretion of pro-calcified EVs. Mechanistically, as a mechanotransducer, the epidermal growth factor receptor (EGFR) initiates the flow-based mechanical cues to MAPK signaling pathway, facilitating the nuclear accumulation of the transcription factor krüppel-like factor 5 (KLF5). Furthermore, pharmacological inhibiting either EGFR or MAPK signaling pathway blocks the nuclear accumulation of KLF5 and finally results in the maintenance of contractile VSMCs even under increased IFSS stimulation. Collectively, targeting this signaling pathway holds potential as a novel therapeutic strategy to inhibit VSMCs phenotypic switching and mitigate the progression of atherosclerosis.

Keywords: phenotype switch, interstitial fluid shear stress, extracellular vesicle, KLF5

Introduction

Cardiovascular diseases (CVDs) remain the leading cause of death worldwide [1]. Atherosclerosis (AS) is a major pathological feature of many CVDs and can lead to myocardial infarction, ischemic cardiomyopathy, stroke, and peripheral arterial disease [2, 3]. Vascular calcification, characterized by

the ectopic deposition of calcium and phosphate crystals in the blood vessel wall, is a prominent feature of advanced atherosclerotic arteries. During the progression of atherosclerotic lesions, vascular smooth muscle cells (VSMCs) undergo phenotype switching, transition from a contractile phenotype,

characterized by markers such as smooth muscle α -actin (α -SMA), smooth muscle protein 22- α (SM22 α), calponin, and myosin heavy chain 11, to a synthetic phenotype. This synthetic phenotype, indicated by markers like matrix metalloproteinase-2 (MMP2), and MMP9, enhances the proliferative and migratory capabilities of VSMCs [4, 5]. This “contractile to synthetic” phenotype transition is a critical factor in the development of atherosclerosis [6]. Current pharmacological treatments primarily target low-density lipoprotein cholesterol, which is associated with major risk factors such as hypercholesterolemia, hypertension, and diabetes [7]. However, these therapies have limited direct impact on the VSMCs per se. Percutaneous coronary intervention with a stent has significantly reduced mortality rates in patients with acute coronary syndromes [8], but the development of neo-atherosclerosis, also known as in-stent restenosis, has emerged as a major safety concern due to the increased proliferative VSMCs resulting from phenotypic switching [9]. Therefore, directly targeting the phenotypic switching of VSMCs holds therapeutic promise, particularly for patients with CVDs who have relatively normal cholesterol levels, those who experience recurrent CVDs despite lipid-lowering therapy, and those who develop in-stent restenosis after coronary stent implantation.

In healthy vasculature, biomechanical forces play a fundamental role in regulating signaling and gene expression, maintaining vascular homeostasis, and ensuring optimal vascular function [10]. Axial stress from longitudinal stretching and circumferential stress generated by cyclic strain induce these forces. Such mechanical stimuli have been found to trigger the release of vasoactive substances, including nitric oxide (NO), through the phosphatidylinositol-3-OH kinase (PI3K)/Akt pathway and Ca^{2+} /calmodulin signaling [11]. Additionally, these mechanical forces influence the diffusion and modulation of various chemokines and cytokines within VSMCs. In a healthy artery with intact endothelial coverage on the intimal layer, medial VSMCs do not sense changes in wall shear stresses caused by blood flow. Instead, they perceive transmural interstitial flow driven by the transmural pressure gradient [12]. However, in the presence of endothelial damage in an atherosclerotic artery, VSMCs are exposed to elevated transmural pressure gradients, leading to increased interstitial fluid shear stress (IFSS) caused by heightened interstitial flow. IFSS has been identified as a regulator of various VSMCs behaviors [10, 12-14]. Research has shown that the surface glycocalyx mediates VSMCs contraction and inhibits proliferation upon IFSS

stimulation [13, 15]. However, accurately measuring the precise value of IFSS experienced by VSMCs remains a challenge, limiting research investigating the contribution of IFSS to VSMCs phenotypic switching. As a result, the molecular mechano-transduction process through which IFSS mediates VSMCs phenotypic switching remains unclear.

Synthetic VSMCs actively participate in intimal calcification through various mechanisms, including apoptosis, osteo/chondrogenic trans-differentiation, and cellular senescence [16-18]. Extracellular vesicles (EVs) are membrane-bound microparticles released by cells and are crucial for cell-to-cell communication, transferring molecules like proteins and RNA, which significantly impact physiological and pathological processes. It is well-known that they are key players in diseases such as cancer, cardiovascular diseases, and neurodegenerative disorders, making them potential biomarkers for diagnosis and prognosis [19]. Additionally, their therapeutic potential is being explored in drug delivery and regenerative medicine due to their natural cargo-carrying capabilities, biocompatibility, and role in immune system modulation [19]. Recent evidence suggests that EVs derived from synthetic VSMCs play a significant role in mediating intimal calcification [20]. These EVs are released into the extracellular space and provide nucleation sites for vascular calcification. Conversely, EVs derived from platelet induced VSMCs migration and proliferation [21]. Therefore, there likely exists a complex interplay between VSMCs phenotypic switching and EVs secretion, necessitating further research to elucidate the specific mechanisms involved. On the other hand, some literatures suggested that there is a correlation between mechanical stress and EVs biogenesis. For instance, the release of microparticle, a kind of EVs, are inhibited by higher shear in endothelial cells. The loading of cyclic stretch on VSMCs has discrepancies on EVs yield. 18% cyclic stretch (at 1 Hz) increases 2- and 3-fold EVs production in VSMCs [22], while 12% cyclic stretch (at 1 Hz) loading does not show changes in EVs production [23]. However, it cannot be refrained from posing the question that what the role of increased IFSS plays in the VSMCs-derived EVs secretion.

In this study, we directly examined human samples from both healthy individuals and patients with atherosclerosis, establishing a direct connection to the disease. Our investigation revealed a clear association between the “contractile to synthetic” phenotype switching of VSMCs and the significant release of EVs in atherosclerotic tissues. To accurately evaluate the impact of increased IFSS, we employed numerical simulations incorporating parameters

including fluid viscosity, dynamic viscosity, and porosity, representing different layers of the artery. Subsequent *in vitro* validation confirmed the pivotal role of IFSS in regulating VSMCs phenotypic switching. Notably, there is a substantial increase in EV release following VSMCs phenotypic switching, thus promoting vascular calcification. Mechanistically, the transcriptional factor krüppel-like factor 5 (KLF5) accumulated in the nucleus of VSMCs after exposure to increased IFSS. Blocking KLF5 conversion restored synthetic VSMCs to the contractile state even under elevated IFSS stimulation. Furthermore, our research conclusively establishes the membrane-bound receptor epidermal growth factor receptor (EGFR) and its downstream MAPK signaling pathway as the upstream regulator of KLF5, mediating the transduction of flow-based mechanical cues. This work highlights the central role of EGFR-MAPK-KLF5 signaling in the mechanosensory transduction machinery that drives IFSS-induced phenotypic switching of VSMCs. This knowledge provides valuable insights into potential therapeutic targets for inhibiting VSMCs phenotypic switching in the treatment of atherosclerosis, offering a novel avenue for intervention in this disease.

Materials and Methods

Human Artery Samples

Normal artery tissue samples were obtained from heart transplant donors, while atherosclerotic artery tissue samples were collected from heart transplant recipients. The collection process strictly adhered to approved guidelines and obtained informed consent from all participating individuals. The study received ethical approval from the institutional Medical Ethics Committee, ensuring compliance with ethical standards.

Cell Cultures

Human aortic smooth muscle cells (HASMCs, ScienCell) were cultured in Smooth Muscle Cell medium (SMCM, ScienCell), which consists of 500 mL of basal medium, 10 mL of fetal bovine serum (FBS), 5 mL of smooth muscle cell growth supplement, and 5 mL of penicillin/streptomycin solution. The cells were maintained in a 5% CO₂ humidified incubator at 37 °C with the medium-replenished every two days. For calcified HASMCs culturing, the osteogenic induction medium (OM) is employed. OM, comprised of high-glucose Dulbecco's Modified Eagle Medium (DMEM), is supplemented with 10% FBS, 1% dual antibiotics, 10 mM β-glycerophosphate, 50 μg/mL ascorbic acid, and 100 nmol/L dexamethasone. Heparin (200 U/mL for 5 days) was used to maintain the contractile phenotype, setting up as the negative

control. Additionally, the HASMCs subjected to PDGF-BB (20 ng/mL for 1 day) were used to mimic the synthetic phenotype and regarded as positive control.

Animals

C57BL/6 mice and apolipoprotein E-deficient (*ApoE*^{-/-}) mice were procured from DOSSY Experimental Animal Co., LTD. The animal study was conducted in accordance with the guidelines set by the China Council on Animal Care and was approved by the Medical Ethics Committee of Sichuan University. The C57BL/6 mice were housed in standard cages with a normal diet and unrestricted access to water and maintained under a 12 h light/dark cycle. On the other hand, the atherosclerotic *ApoE*^{-/-} mice were fed a high-fat diet for 12 weeks [24]. Before the experiments, all mice underwent a minimum of three days of acclimatization. They were housed at a temperature of 20 ± 2°C with 50% ± 10% humidity while being protected from ultraviolet light, noise, and strong odors.

Calculation of Interstitial Fluid Shear Stress

Blood vessels were collected from both control and atherosclerosis (AS) patients and preserved in 4% paraformaldehyde. Afterward, the vessels were embedded in paraffin, cross-sectioned, and subjected to HE staining. The staining results were used to measure the thickness and porosity of the inner, middle, and outer layers of the vessels. Additionally, an idealized computational model of blood vessels has been established. The internal diameter of the vessel was set at 19 mm [25], with a length of 100 mm [26], to ensure adequate fluid flow. In this study, the structured grid is used to divide the model, and the boundary layer is added to the fluid-solid interface, and the final grid number is 1.43×10⁶. Computational fluid dynamics (CFD) is used to calculate the steady state, and CFD simulation is carried out by using commercial software Ansys Fluent. The incompressible N-S equation is solved by SIMPLE method, and the calculation is considered to be convergent when the residual is less than 10⁻⁵ and the difference between the outlet and inlet mass flows is less than 0.01% of the outlet mass flow. The simulation calculation uses steady-state calculation, so the time step is not involved.

The N-S equation is as follows:

$$\nabla u = 0 \quad (1)$$

$$\rho \left(\frac{\delta u}{\delta t} \right) + \rho u \cdot \nabla u = \nabla [-pI + \mu(\nabla u + (\nabla u)^T)] + F \quad (2)$$

Where the blood velocity (*u*), pressure (*p*), dynamic viscosity (*μ*), blood density (*ρ*), and volume

force field (F) play crucial roles in understanding the mechanics of blood flow. The blood density was determined as $1.05 \times 10^3 \text{ kg/m}^3$, and the viscosity was $0.0035 \text{ Pa}\cdot\text{s}$. The interstitial flow had a density of $1.0 \times 10^3 \text{ kg/m}^3$ and a viscosity of $0.0035 \text{ Pa}\cdot\text{s}$ [27]. The vessel wall was modeled as a porous media. The inlet boundary conditions were defined by a lumen blood flow velocity of 5 L/min and an interstitial flow velocity ranging from $0.1\text{-}1.0 \text{ }\mu\text{m/s}$ [28]. The outlet boundary conditions were set at an intraluminal pressure of 70 mmHg [29]. Physiological/pathological parameters and boundary conditions used in the numerical model are listed in Table 1. The thickness and porosity of the vascular model are all measured according to the HE staining of human vascular samples, which are detected by FIJI ImageJ (Version 1.53).

Table 1. Physiological/Pathological parameters and boundary conditions used in the numerical model.

Layers	Parameters	Normal	Atherosclerosis
Lumen	Diameter, mm	19	19
	Density ρ , g/mm ³	1.05×10^{-3}	1.05×10^{-3}
	Dynamic viscosity μ , g/(mm·s)	3.5×10^{-3}	3.5×10^{-3}
	Inlet flow, L/min	5	5
	Outlet pressure, mmHg	70	70
Endothelium	Thickness, μm	182.2	209.5
	Density ρ , g/mm ³	1.05×10^{-3}	1.05×10^{-3}
	Dynamic viscosity μ , g/(mm·s)	3.5×10^{-3}	3.5×10^{-3}
	Porosity ϵ	0.054	0.122
Smooth Muscle Cell	Thickness, μm	1234.6	1220.33
	Density ρ , g/mm ³	1.00×10^{-3}	1.00×10^{-3}
	Dynamic viscosity μ , g/(mm·s)	3.5×10^{-3}	3.5×10^{-3}
	Porosity ϵ	0.05	0.08
	Interstitial flow velocity, $\mu\text{m/s}$	0.1/1	0.1/1
Adventitia	Thickness, μm	162.1	248.6
	Density ρ , g/mm ³	1.05×10^{-3}	1.05×10^{-3}
	Dynamic viscosity μ , g/(mm·s)	3.5×10^{-3}	3.5×10^{-3}
	Porosity ϵ	0.01	0.01

In the CFD calculation, the model is simplified to a certain extent, and the specific value is the average value of the wall shear stress (WSS) at the interface between the endothelial cell layer and the smooth muscle cell layer. The WSS is the projection of the traction vector in the direction tangent to the wall [30].

$$WSS = n_w \cdot \tau \cdot n_s^T$$

where $n_w = n_r e_r + n_z e_z$ is the unit normal vector to the surface of interest. τ is the Cauchy stress tensor, $n_s = -n_z e_r + n_r e_z$ is the unit vector tangent to the wall surface. The surface traction vector, $T = n_w \cdot \tau$ is the inner product of the Cauchy stress tensor and the unit normal vector to the surface of interest.

IFSS Loading Condition

The IFSS loading system utilized in this study consisted of a parallel plate flow chamber and a

peristaltic pump system (Masterflex model 7518-10, Cole-Parmer Instrument Company). HASMCs were exposed to IFSS in this loading system. The calculation of the loading shear stress was based on a previously described formula [31]:

$$\tau = 6 \frac{\mu Q}{H^2 W}$$

In the formula, τ represents the IFSS applied to the cells; μ ($0.83 \text{ mPa}\cdot\text{s}$) represents the viscosity of the circulating buffer; Q represents the velocity of the flow; H (0.4 mm) represents the height of the chamber; and W (95 mm) represents the width of the chamber. According to the above formula, when τ is set at 0.5 or 3 dyn/cm^2 , the corresponding Q value is 9 or 55 mL/min , respectively. During the 8 h IFSS loading process, the loading system was placed in a 37°C , $5\% \text{ CO}_2$ incubator. To investigate the role of EGFR and MAPK signaling pathway, HASMCs were pretreated with the EGFR inhibitor gefitinib ($1 \text{ }\mu\text{M}$) for 48 h and MEK inhibitor PD9805 ($10 \text{ }\mu\text{M}$) for 24 h before IFSS loading.

Statistical Analysis

To minimize potential environmental bias or unintentional error, quantitative experiments were performed at least three times. SigmaPlot software (Systat, Erkrath) was used for statistical analyses. Depending on the results of the Shapiro-Wilk test for normal distribution, either Student's t-test or the non-parametric Mann-Whitney U rank sum test was used for statistical analysis. The error bars in the bar graphs represent the standard errors of the mean (SEM). In the figures and legends, the corresponding P values are indicated by symbols such as * $P < 0.05$, ** $P < 0.01$, *** $P < 0.001$, and n.s. for no significance. GraphPad Prism 8.0 software (La Jolla) was used to generate the graphs.

Results

The Phenotypic Switching of VSMCs Is Accompanied by an Increase of EVs in the Atherosclerotic Artery

To begin, we conducted a comprehensive analysis to confirm the occurrence of phenotypic switching in VSMCs within human atherosclerotic artery tissue. Utilizing confocal imaging, we observed a notable increase in the expression of synthetic marker matrix metalloproteinase-9 (MMP9), accompanied by a decline in the contractile marker alpha-smooth muscle actin ($\alpha\text{-SMA}$) in the atherosclerotic artery tissue (Figure 1A and 1B). We further validated this relationship in an *ApoE*^{-/-} mouse atherosclerotic model, which is characterized by abundant lipid deposition in the different artery

segments (Figure S1A and S1B). Consistently, phenotypic switching of VSMCs was observed in the media layer leading to a narrowed artery lumen (Figure S1C-G). The artery consists of layers including the intima, media, and adventitia, each populated with diverse cells and extracellular matrix

proteins, notably elastin and collagens in the media layer, the site of VSMCs [32]. The blue, long, wavy structures observed in the media layer in Figures 1A and 1C likely result from the nonspecific staining of the elastic lamina.

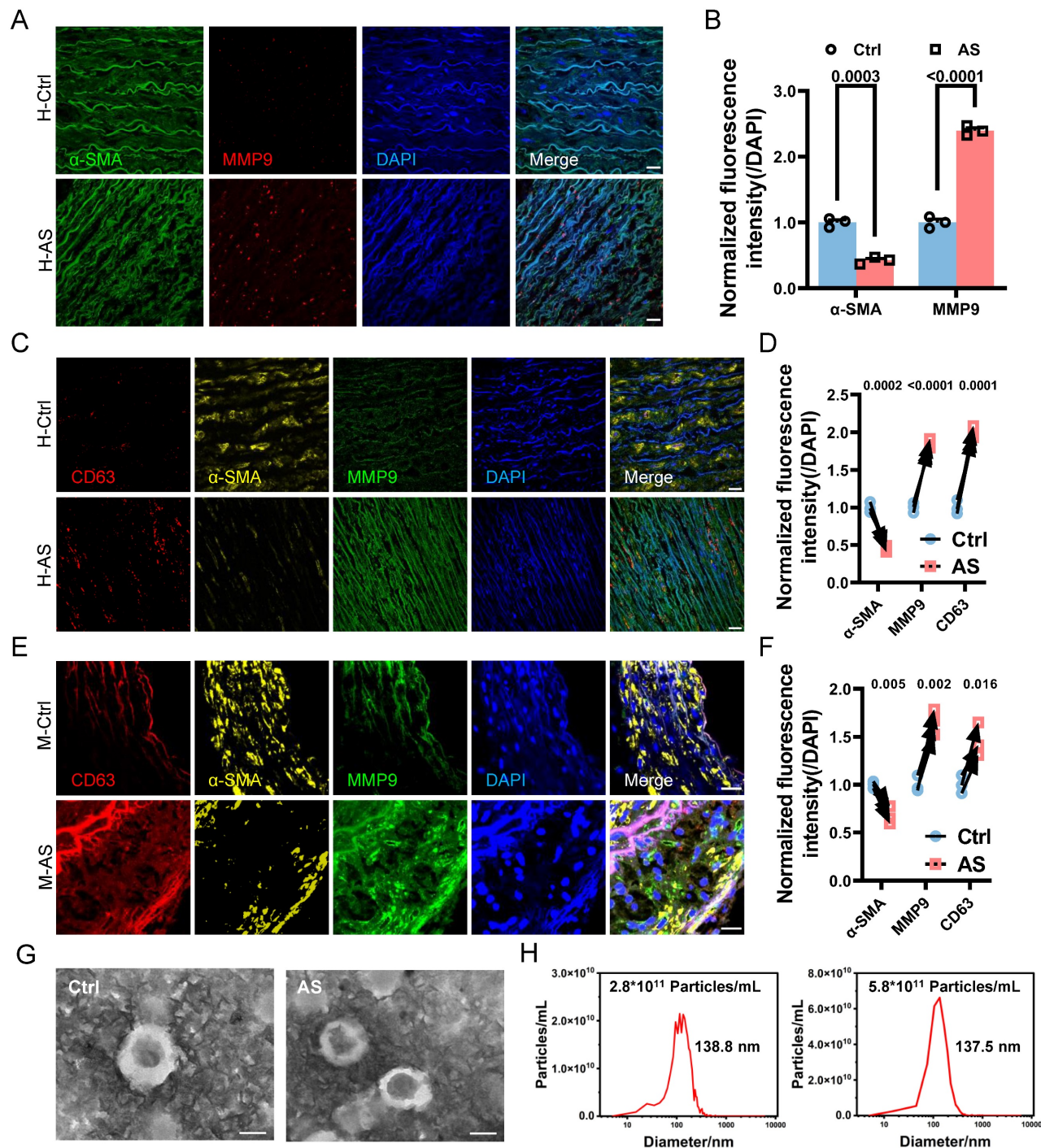


Figure 1. Phenotypic switching of VSMCs is associated with increased EVs in atherosclerotic plaque. (A, B) Immunostaining and the normalized intensities show the expression change of phenotype switching indicators in VSMCs from the atherosclerosis plaque, α -SMA (the contractile marker, red), MMP9 (synthetic marker, green), and DAPI (nucleus, blue). Scale bar, 20 μ m, n=3. (C) Immunostaining exhibits the location and expression of VSMCs phenotype (α -SMA, yellow, MMP9, green) and extracellular vesicles markers (CD63, red) in human atherosclerotic arteries. Nuclei were counterstained with DAPI (blue). Scale bar, 20 μ m, n=3. (D) Correlation analysis of VSMCs phenotypic switching markers and EVs markers. (E, F) The expression and correlation analysis of VSMCs phenotype and extracellular vesicles markers in the mouse atherosclerotic artery (α -SMA, yellow, MMP9, green, CD63, red). Nuclei were counterstained with DAPI (blue). Scale bar, 20 μ m, n=3. (G) The released EVs from the representative normal and atherosclerotic mouse artery tissue are harvested and identified by the TEM analysis. Scale bar, 100 μ m, n=6. (H) NTA analysis is used to determine the particle size and number of the EVs harvested in (G). Data are presented as mean \pm SEM, and statistical analysis was performed by a two-tailed unpaired t-test.

Given the growing evidence implicating EVs in the development and progression of atherosclerosis [33], we further evaluated the secretion of EVs in the atherosclerotic artery. Comparative analysis between normal human arteries and atherosclerotic arteries revealed a significant increase in the colocalization of VSMCs phenotypic switching and the EVs marker CD63 in the atherosclerotic artery (**Figure 1C and 1D**). Similarly, phenotypic switching VSMCs in the atherosclerotic mouse aortic arch also exhibited a higher expression level in CD63 (**Figure 1E and 1F**). This positive correlation between CD63 expression and VSMCs phenotypic switching was also observed in other artery segments of atherosclerotic mice (**Figure S2 A-D**).

To further verify the association between VSMCs phenotypic switching and increased EV release, we performed transmission electron microscopy (TEM) and nanosight tracking analysis (NTA) to characterize and accurately quantify EVs in the atherosclerotic artery. The isolated EVs exhibited the typical double-layered cup-shaped structure (**Figure 1G**) and size distribution (**Figure 1H**) in both normal and atherosclerotic mouse arteries. However, the EVs amount in atherosclerotic mouse artery (5.8×10^{11} particles/mL) was significantly higher than that in normal mouse artery (2.8×10^{11} particles/mL), with a ratio approximately reaching 2.1. These findings strongly suggest that VSMCs undergo phenotypic switching in atherosclerosis, accompanied by an increased release of EVs.

Increased Interstitial Fluid Shear Stress Drives VSMCs Phenotypic Switching

The phenotypic switching of VSMCs is known to be responsive to various pathological stimuli, including pro-inflammatory cytokines and biomechanical factors [4]. In the context of atherosclerosis progression, the damaged endothelium leads to the modulation of various VSMCs behaviors through increased IFSS [10, 12, 13]. However, it remains unclear whether increased IFSS directly regulates phenotypic switching. Furthermore, the accurate measurement of IFSS *in vivo* poses a challenge, leading to a debate regarding its precise value when VSMCs are exposed to it within the atherosclerotic artery. To address these issues, we performed immunofluorescent staining to detect the endothelial layer remodeling and vascular morphology changes in the atherosclerotic artery. Both human and mouse samples of atherosclerotic arteries exhibited irregular endothelial cell arrangement, a loose structure, and the formation of numerous pores (indicated by white arrows) compared to normal arteries (**Figure 2A and 2B**). This

observation was further confirmed by the HE staining of artery tissue (**Figure 2C**). Quantification of artery porosity based on histological staining revealed an increase from 5.4% to 12.2% in the intimal layer (**Figure 2D**), and from 5.0% to 8% in the medial layer (**Figure 2E**) in atherosclerotic arteries. Although the internal elastic lamina prevented the blood flow from seeping into the medial layer [34], the increased permeability of endothelium and enlarged porosity of the medial layer resulted in an elevated interstitial flow near the intima layer with a gradually reduced tendency (**Figure 2F**). To determine the precise magnitude of IFSS, we performed numerical calculations of interstitial flow near the intima layer, which is highlighted by dark circle in **Figure 2G** and **2H** (left panel), based on the physiological and atherosclerotic parameters and boundary conditions (detailed information in **Table 1**). Interstitial fluid velocity was set within the range of $0.1 \mu\text{m/s}$ to $1 \mu\text{m/s}$ [35, 36]. Consequently, we determined that the precise magnitude of IFSS in normal arteries ranged from 0.06 to 0.6 dyn/cm^2 , while in atherosclerotic arteries, it ranged from 0.33 to 3.27 dyn/cm^2 (**Figure 2G and 2H**, right panel).

To accurately select the most representative IFSS value regulating phenotypic switching of VSMCs, we utilized the minimum, average, and maximum values derived from our calculations for experimental validation. In addition, heparin was used to maintain the contractile phenotype of VSMCs setting as the negative control group. In contrast, the synthetic VSMCs induced by PDGF-BB were regarded as the positive control group [20, 37]. Immunofluorescence staining revealed that VSMCs do not acquire synthetic phenotype under physiological IFSS ($\leq 0.5 \text{ dyn/cm}^2$) condition. In contrast, VSMCs exposure to pathological IFSS ($\geq 1.5 \text{ dyn/cm}^2$) exhibit a progressive decrease in contraction phenotype markers $\alpha\text{-SMA}$ and $\text{SM22}\alpha$ and a concomitant increase in synthetic phenotype markers MMP9 and MMP2 (**Figure S3A and S3B**). It was supported by the data from western blot assay. Compared with VSMCs upon heparin treatment, the VSMCs subjected to $\text{IFSS} \leq 0.5 \text{ dyn/cm}^2$ do not show significantly different expression of contractile markers (**Figure S3C-E**). Conversely, VSMCs with 3 dyn/cm^2 IFSS exposure show the most obviously decreased expression in contractile markers ($\alpha\text{-SMA}$ and $\text{SM22}\alpha$) and the most remarkably increased expression in synthetic marker (MMP-2). It was consistent with the expression of phenotypic markers in VSMCs cultured in PDGF-BB (**Figure S3C and S3F**). Furthermore, the qRT-PCR assay confirmed the expression change of phenotypic markers at gene level (**Figure S3G-K**). Collectively, VSMCs with 0.5 dyn/cm^2 IFSS stimulation show the most pronounced

characterization of contractile phenotype, while VSMCs subjected to 3 dyn/cm² IFSS have the most likely tendency of synthetic marker with that in VSMCs cultured with PDGF-BB. Therefore, we used 0.5 dyn/cm² IFSS as the physiological group and 3 dyn/cm² IFSS as the pathological group.

Next, we aimed to further verify whether increased IFSS in the medial layer of the atherosclerotic artery is the main driver for VSMCs phenotypic switching *in vitro*. When exposed to increased IFSS stimulation, VSMCs exhibited reduced

expression of the contractile marker α -SMA and increased expression of the synthetic marker MMP9 (Figure 3A-D), indicating that the increased IFSS promoted the phenotypic switching of VSMCs. The elevated motility of VSMCs further confirmed the occurrence of phenotypic switching in response to increased IFSS (Figure 3E and 3F). Moreover, through western blot and qRT-PCR assays, we found that the contractile phenotype markers α -SMA and SM22 α were significantly reduced under 3 dyn/cm² IFSS stimulation, whereas the synthetic phenotype marker

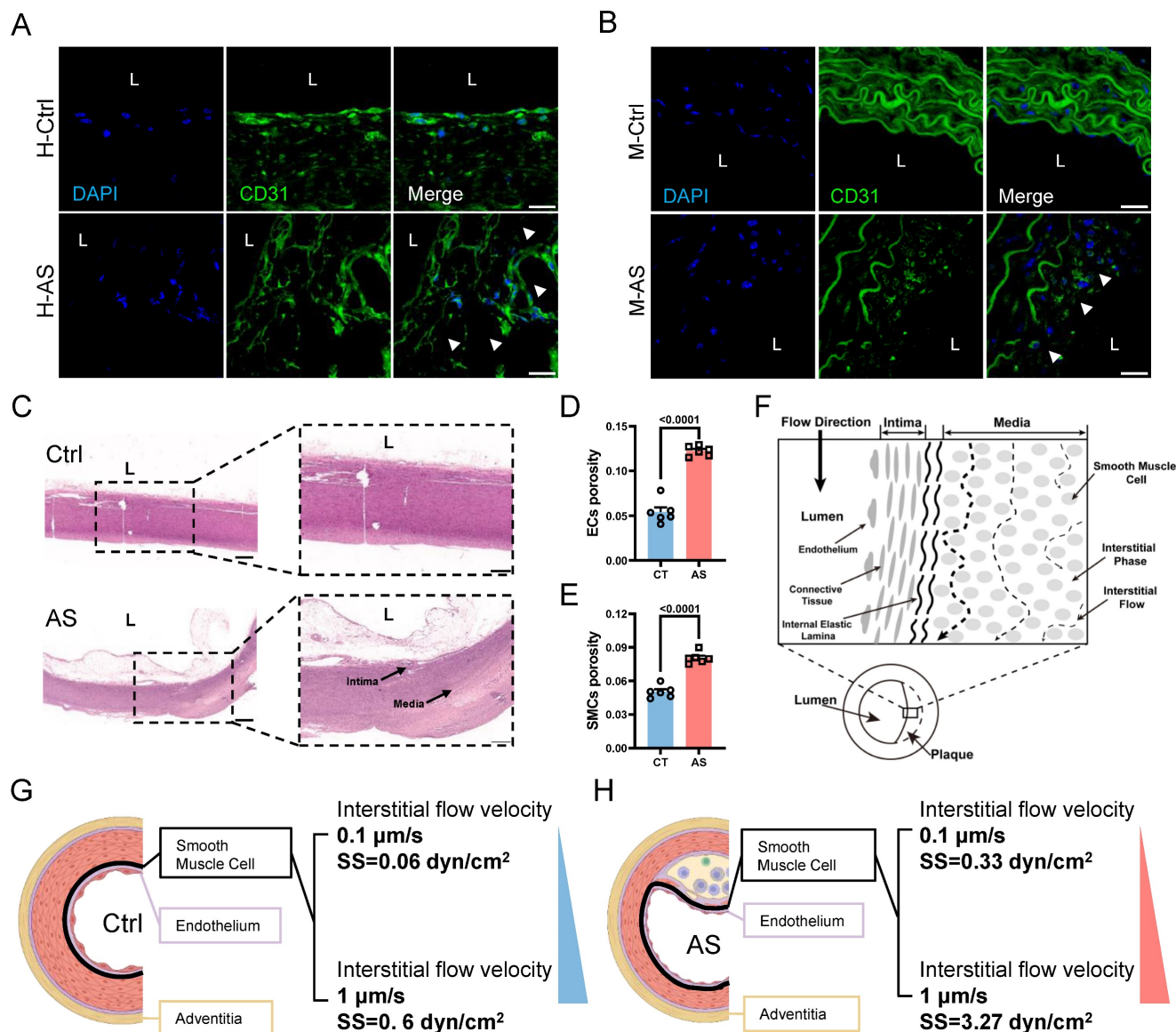


Figure 2. The remodeling of atherosclerotic artery leads to the increased interstitial flow. (A, B) Immunostaining illustrates the remodeling of the intimal and medial layer in the normal and atherosclerotic artery tissues from the representative human (A) and mice (B), respectively. White arrows indicate the impaired endothelial layer. CD31 (endothelial cells indicator, green), nucleus (DAPI, blue), L denotes the vascular lumen. Scale bar, 20 μ m, n=3. (C) HE staining of normal and atherosclerotic arteries from humans reveals the remodeling of the intima and media layers. Scale bar, 500 μ m, n=3. (D, E) Quantification of porosity in the intimal endothelial cells and the medial VSMCs, n=6. Unpaired t-tests were used to compare variables with normal distribution and homogeneity of variance. All data are presented as mean \pm SEM. (F) A schematic diagram of aortic remodeling induced the change of interstitial flow. All three dashed lines represent interstitial flow, with the interstitial flow near the intima layer being the highest (the first black dashed line on the left). (G) Numerical calculation of IFSS subjected to VSMCs in the media layer near the intima layer (thick black line) is based on the physiological parameters of the normal human artery. The inlet flow speed ranges from 0.1 μ m/s to 1 μ m/s and the magnitude of IFSS ranges from 0.06 to 0.6 dyn/cm². SS: shear stress. (H) Numerical calculation of IFSS subjected to VSMCs in the media layer near the intima layer (thick black line) according to the pathological parameters of the atherosclerotic human artery. The inlet flow speed ranges from 0.1 μ m/s to 1 μ m/s and the magnitude of IFSS ranged from 0.33 to 3.27 dyn/cm². SS: shear stress.

MMP2 was significantly upregulated (Figure 3G-O). In summary, we utilized numerical simulations to calculate the values of IFSS and *in vitro* validation

revealed that 0.5 dyn/cm² and 3 dyn/cm² can simulate the IFSS under physiological and pathological conditions for subsequent experiments.

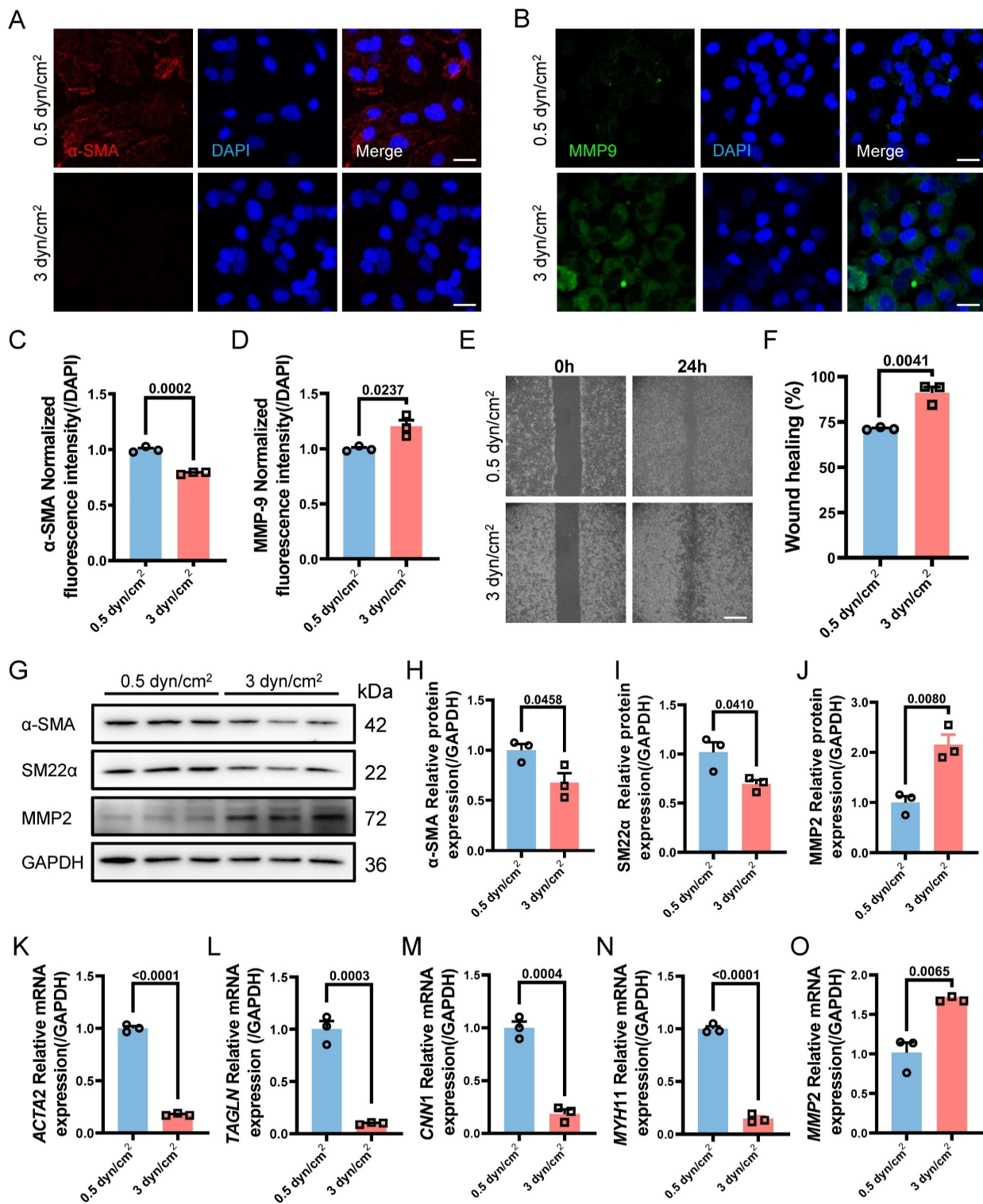


Figure 3. Increased interstitial flow promotes the phenotype switching of VSMCs. (A, B) Immunostaining indicates the expression changes of phenotype markers (A, α -SMA, red), (B, MMP9, green) in HASMCs upon increased IFSS stimulation *in vitro*. The nucleus is counterstained with DAPI (blue). Scale bar, 20 μ m, n=3. (C, D) Normalized fluorescence intensity of α -SMA and MMP9 were quantified in Figure 3A and 3B respectively. (E, F) Wound healing assay verified the increased mobility of HASMCs after phenotypic switching upon IFSS stimulation. Scale bar, 200 μ m, n=3. (G-J) Western blot and quantitative analyses of phenotypic switching indicators in HASMCs exposed to increased IFSS. (K-O) mRNA levels of contractile markers (*ACTA2*, *TAGLN*, *CNN1*, and *MYH11*) and synthetic marker (*MMP2*) in HASMCs after IFSS stimulation. The relative abundances of transcripts were quantified and normalized to *Gapdh*, n=3. Data are presented as mean \pm SEM, and statistical analysis is performed by a two-tailed unpaired t-test.

VSMCs Phenotypic Switching Serves as the Upstream Regulator of EVs Secreting

After determining the specific magnitudes of IFSS *in vitro*, we attempted to observe whether mechanical loading on VSMCs leads to the release of extracellular vesicles. NTA assay showed that the number of EVs from VSMCs subjected to the increased IFSS reached 4.2 times higher than that from VSMCs exposed to normal IFSS (Figure S4A and S4B). We assessed the EVs markers CD63 and TSG101 through western blot (Figure S4C), and also measured the concentration of EVs (Figure S4D and S4E), observing a significant increase in the release of EVs after IFSS loading. Besides, we detected the expression of CD63 through immunostaining and qRT-PCR, both of which demonstrated higher expression of CD63 (Figure S4F-H). Rab27a, a pivotal contributor to EVs biogenesis and secretion, was generally selected to evaluate the release of EVs [38]. It has been shown that silencing Rab27a inhibited the biogenesis of EVs [39]. In line with the previous research, Rab27a exhibited a significant increase in VSMCs after increased IFSS stimulation (Figure S4I-K). These results drew our attention, the elevated IFSS could also induce the releasing of EVs-derived from VSMCs.

VSMCs undergo phenotypic switching and secrete EVs in response to increased IFSS in the atherosclerotic artery. The relationship between VSMCs phenotypic switching and EVs secretion remains unclear, as both factors have been shown to influence each other's functions. Low-density lipoprotein (LDL) particles have been shown to promote EVs release from VSMCs into the adjacent tissue [40]. Conversely, EVs also influence VSMCs phenotypic switching, thereby contributing to abnormal VSMCs proliferation [41]. Subsequently, we sought to unravel the upstream regulator between the two under increased IFSS conditions. Firstly, heparin was used to maintain the contractile phenotype of VSMCs. This treatment group was regarded as the negative control group to compare the physiological simulating efficiency of 0.5 dyn/cm² for keeping VSMCs quiescence. Distinctly, the elevated amount of EVs from VSMCs induced by increased IFSS was observed (Figure 4A-F), while 0.5 dyn/cm² and heparin groups do not show the increased EVs. It suggested that the contractile phenotype of VSMCs suppresses the release of EVs from VSMCs.

On the other hand, we established a synthetic phenotype model of VSMCs by using PDGF-BB [37] and extracted EVs from both the PDGF-BB or increased IFSS-induced synthetic VSMCs. Co-culturing VSMCs with EVs derived from either the PDGF-BB-induced or the increased IFSS-induced

synthetic VSMCs did not induce phenotypic switching of the recipient cells (Figure 4G-I). Furthermore, the western blot analysis revealed that the expression of synthetic phenotype markers marker MMP2 and contractile markers (α -SMA, SM22 α) did not show a significant change in VSMCs exposed to EVs derived from synthetic VSMCs (Figure 4J-M). These results suggest that EVs-derived from the synthetic VSMCs may be incapable of inducing VSMCs phenotypic switching. Collectively, VSMCs phenotypic switching acts on the upstream regulator of EVs secreting.

Based on the above results, another interesting question arises: what is the function of EVs-derived from the synthetic VSMCs induced by increased IFSS? Our subsequent objective was to assess the impact of EVs-derived from the synthetic VSMCs under increased IFSS in the development of atherosclerosis. Vascular calcification is a common feature observed in different stages of the atherosclerotic plaque [42]. Consistently, we observed significant calcified nodes in human atherosclerotic artery tissue (Figure 5A and 5B), aortic arch segments (Figure 5C and 5D) and other artery segments of atherosclerotic mice (Figure 5S A-F). The co-localization of EVs with synthetic VSMCs in atherosclerotic arteries suggests that the EVs may play a potential promoter of vascular calcification. To investigate this hypothesis, we isolated EVs from primary VSMCs of the atherosclerotic mouse artery and co-cultured with the primary VSMCs from the normal mouse artery. The results exhibited an increase in calcified nodules following exposure to these EVs, as observed through alizarin red staining (Figure 5E and 5F). Additionally, *in vitro*, the EVs derived from VSMCs under increased IFSS accelerate the higher expression of calcified markers (RunX2 and ALP) in normal VSMCs (Figure 5G-I), suggesting the pro-calcification role of these EVs. These results collectively demonstrated that the EVs derived from synthetic VSMCs do not induce phenotypic switching of recipient VSMCs but do initiate the calcification of VSMCs. Given that increased IFSS triggers phenotypic switching of VSMCs, we hypothesize that increased IFSS serves as the initial factor in vascular calcification during the progress of atherosclerosis.

Transcription Factor KLF5 is the Executor for VSMCs Phenotypic Switching

Given the involvement of the increased IFSS in VSMCs phenotypic switching and calcification, our subsequent objective was to investigate the underlying biomechanical mechanisms responsible for the induction of VSMCs phenotypic switching by increased IFSS. We performed transcriptome

sequencing of VSMCs exposed to increased IFSS. In comparison to VSMCs under normal IFSS, the volcano plot exhibited 393 upregulated and 385 downregulated genes in VSMCs upon increased IFSS stimulation (**Figure 6A**). Gene ontology enrichment analysis showed that increased IFSS influences cell proliferation, metabolism, and differentiation, all of which are tightly associated with phenotypic switching [5] (**Figure S6A**). These data further support the critical role of increased IFSS in initiating VSMCs phenotypic switching.

Transcription factors (TFs) and co-transcription factors (co-TFs) directly regulate gene transcription by binding to the promoter region of the target genes, finally resulting in the expression change [43]. To identify the TFs and co-TFs involved in IFSS-induced VSMC phenotypic switching, we conducted a Venn analysis by comparing the differentially expressed genes with known human TFs and co-TFs (**Figure 6B**). Notably, KLF5 exhibited the most significant increase among the differentially expressed TFs and co-TFs associated with phenotypic switching of VSMCs (**Figure 6C**), suggesting its potential role in driving phenotypic switching of VSMCs upon increased IFSS stimulation. This observation was supported by the high expression of KLF5 in the human atherosclerotic artery (**Figure 6D** and **6E**) and the mouse atherosclerotic artery (**Figure S6B**). To further elucidate whether KLF5 responds to increased IFSS after atherosclerosis initiation, we applied 3 dyn/cm² shear stress on VSMCs and examined the expression change of KLF5. Elevated expression and nuclear accumulation of KLF5 were observed in VSMCs subjected to increased IFSS (**Figure 6F** and **6G**). Moreover, both the protein and mRNA levels of KLF5 were significantly increased (**Figure 6H-J**). It is known that the transcriptional activation of KLF5 is regulated by its nuclear shuttling and reduced expression in the cytoplasm [44]. In VSMCs subjected to increased IFSS, the expression levels of cytoplasmic and nuclear KLF5 positively correlated with the magnitude of IFSS (**Figure 6K-N**), and an increased ratio of nuclear/cytoplasmic KLF5 was detected (**Figure 6O**). Taken together, these findings indicate that KLF5 is responsive to increased IFSS in the atherosclerotic artery.

We further investigated whether KLF5 regulates VSMCs phenotypic switching in response to increased IFSS. We generated a KLF5 knockdown cell line (referred to as shKLF5-HASMCs) using shRNA technology and confirmed the knockdown efficiency through western blot and qRT-PCR assay. Remarkably, KLF5 expression was significantly decreased at both the protein and mRNA levels (**Figure S6C-F**). As anticipated, inhibiting KLF5

reverses the decreased expression of contractile markers in VSMCs exposed to increased IFSS. However, the synthetic marker MMP2 did not increase in the shKLF5-HASMCs after increased IFSS exposure (**Figure S6G-J**). Immunostaining also indicated that another synthetic marker, MMP9, remained constant in shKLF5-HASMCs even when subjected to increased IFSS (**Figure S6K-M**). Intriguingly, at the gene level, the expression of contractile markers (*ACTA2*, *TAGLN*, and *CNN1*) was restored in shKLF5-HASMCs subjected to increased IFSS (**Figure S6N-P**). Conversely, deficiency in KLF5 mitigated the expression of the synthetic marker MMP2 in VSMCs exposed to the increased IFSS (**Figure S6Q**). In summary, our findings demonstrate that the transcription factor KLF5 regulates the phenotypic switching of VSMCs.

The Nuclear Accumulation of KLF5 Is Dependent on the MAPK Signaling Pathway

To elucidate the activation of KLF5 by increased IFSS, leading to VSMCs phenotypic switching, we conducted KEGG pathway analysis based on the transcriptome sequencing results. Remarkably, the MAPK signaling pathway was found both in the top ten up-regulated and down-regulated KEGG pathway analysis, emerging as the most potent regulator of KLF5 activation (**Figure 7A**). To investigate this further, we examined the expression of the extracellular signal-regulated kinase (ERK), a downstream component of the classical MAPK signaling pathway [45], in VSMCs exposed to 3 dyn/cm² IFSS. We observed a constant tendency in ERK expression accompanied by enhanced phosphorylated ERK (*p*-ERK) (**Figure 7B** and **7C**). Immunostaining demonstrated this expression tendency as well and showed the nuclear translocation of *p*-ERK in VSMCs after 3 dyn/cm² IFSS loading (**Figure 7D-F**, indicated by white arrows). Subsequently, PD98059 inhibitor was employed to suppress the activation of MAPK signaling pathway under increased IFSS stimulation. After exposure to PD98059, the key components of the MAPK signaling pathway (Ras, Raf, ERK and *p*-ERK) significantly declined in VSMCs even subjecting to increased IFSS (**Figure S7A-D**). Accordingly, the nuclear outward shuttling of *p*-ERK, which was inhibited by PD98059, further confirmed the repression of MAPK pathway activation in IFSS-stimulated VSMCs (**Figure S7E** and **S7F**). These data together led us to explore whether the MAPK signaling pathway could activate KLF5 to initiate VSMCs phenotypic switching. Inhibition of the MAPK signaling pathway with the PD98059 inhibitor resulted in decreased KLF5 expression in VSMCs subjected to increased IFSS (**Figure 7G** and **7H**).

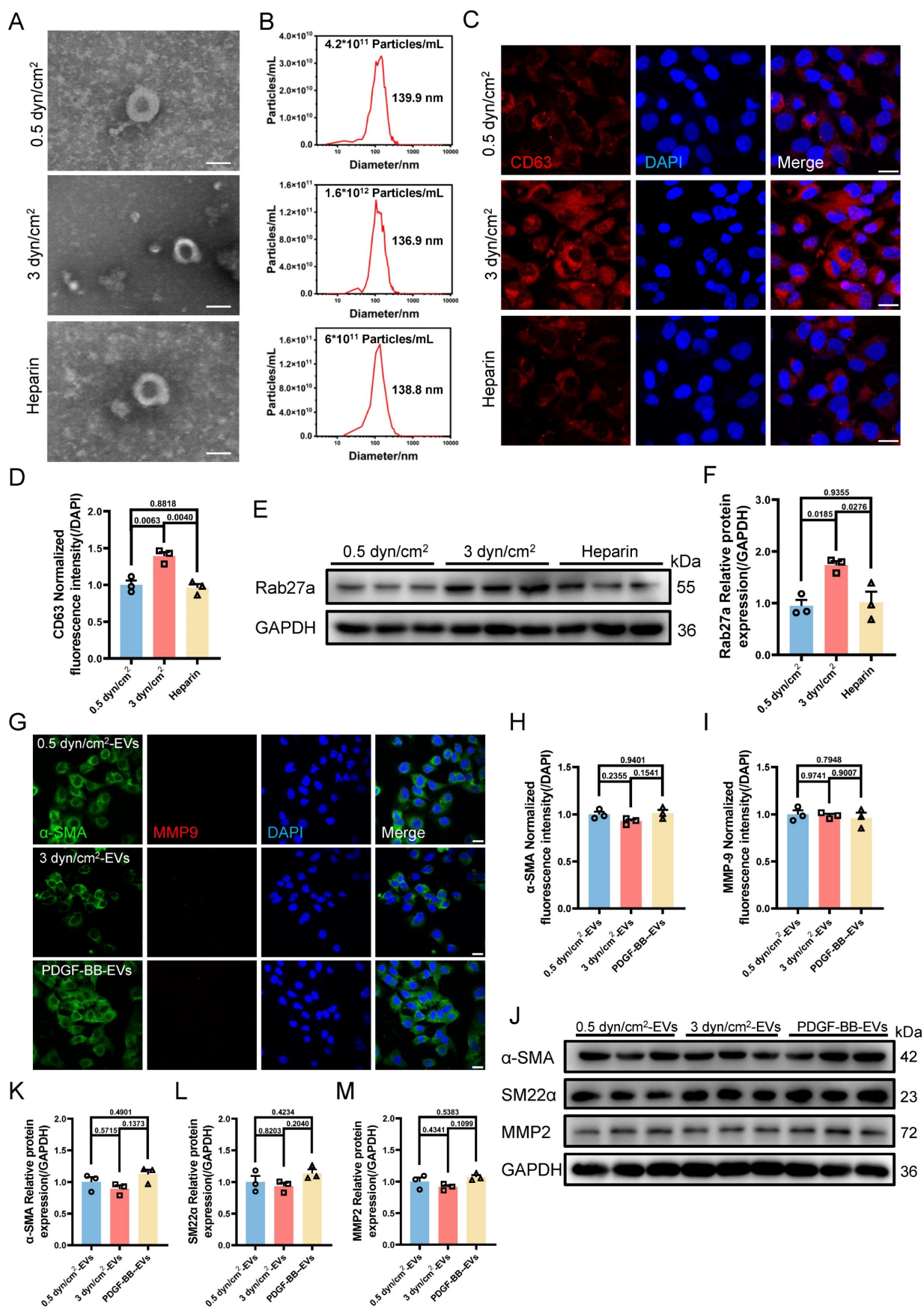


Figure 4. The increased IFSS-induced phenotypic switching of VSMCs is the upstream factor facilitating the EVs release. **(A)** TEM analysis is used to identify the HASMCs-derived EVs after increased IFSS stimulation. Heparin is used to maintain the contractile phenotype of HASMCs. Scale bar, 100 μm. **(B)** NTA analysis measured the size and particle number from HASMCs subjected to the indicated stimulation. **(C, D)** Immunostaining and normalized fluorescence intensity analyses reveal the expression of

CD63 in HASMCs under the indicated stimulation. CD63, red. DAPI was used to stain nuclei (blue). Scale bar, 20 μm , $n=3$. (E, F) Immunoblotting and quantitative analysis of Rab27a in HASMCs after indicated stimulation. GAPDH is used as a loading control, $n=3$. (G-I) Immunostaining and normalized fluorescence intensity analysis illustrate the phenotypic switching of HASMCs after increased IFSS stimulation. PDGF-BB is co-cultured with HASMCs 8 h and induces the synthetic phenotype of HASMCs. α -SMA (green), MMP9 (red). DAPI was used to stain nuclei (blue). Scale bar, 20 μm , $n=3$. (J-M) Immunoblotting and quantitative analysis of phenotypic switching markers in HASMCs with exposure to HASMCs-derived EVs upon the different IFSS stimulation. GAPDH is used as a loading control, $n=3$. Data are shown as mean \pm SEM, and statistical analysis was performed by one-way analysis of variance followed by the Tukey test.

Additionally, immunostaining shows that blocking MAPK signaling pathway excludes the KLF5 from the nucleus in increased IFSS-exposed VSMCs (Figure 7I and 7J). This immunostaining results was confirmed by the western blot assay for KLF5 in the nuclear fraction of VSMCs subjected to increased IFSS (Figure 7K-N), indicating that KLF5 nuclear accumulation is dependent on the MAPK signaling pathway. Next, we evaluated the phenotypic switching of VSMCs after inhibiting MAPK upon IFSS stimulation. The contractile markers (α -SMA and SM22 α) showed remarkably elevated expression, while the synthetic marker (MMP9) exhibited declined expression in VSMCs subjected to PD98059 exposure even with stimulation of increased IFSS (Figure 7O-R, Figure S7G and S7H). These results provide solid evidence that the MAPK signaling pathway is central for the IFSS-induced VSMCs phenotypic switching.

EGFR Initiates the Increased IFSS-based Mechanical Cues Transducing to MAPK Signaling

Our findings underscore the critical role of the MAPK-KLF5 signaling axis in VSMC phenotype switching. It raises another interesting question: how is IFSS signaling propagated from the exterior of the VSMC cell to the nucleus interior? Based on RNA sequence data, we identified 26 differently expressed genes linked to membrane proteins and 14 genes exhibited significant upregulation after increased IFSS stimulation (Figure 8A). Among them, three genes—*EREG*, *SPRY2*, and *PTGER4*—were found to associate with the epidermal growth factor receptor (EGFR), which has been identified as a mechano-transduction mediator [46, 47]. Subsequently, these three genes were validated by qPCR, aligning with sequencing data (Figure S8A-C), suggesting that EGFR is the potential candidate sensing the IFSS-based mechanical clue. After focusing on EGFR, we accordingly performed immunofluorescence staining of phosphorylated EGFR (*p*-EGFR) and EGFR using patient and mouse samples respectively (Figure 8B and S8E). The phosphorylation of EGFR refers to its activation [48]. Interestingly, the elevated *p*-EGFR was observed in the AS group consisting with a reduced α -SMA expression both in the human and mouse samples while EGFR remains stable (Figure S8D and S8F). It indicates that EGFR is activated in the synthetic VSMCs. Furthermore, we conducted an

immunostaining assay to determine whether EGFR is activated in synthetic VSMCs mediated by increased IFSS. Upon increased IFSS stimulating, *p*-EGFR shows a remarkably higher expression while EGFR does not show an increased expression (Figure 8C and 8D). Western blot assay was used to confirm the immunostaining data. The results show that *p*-EGFR has a remarkably higher expression while EGFR remains a stable expression, which resulting in a higher ratio of *p*-EGFR/EGFR (Figure 8E and 8F). The above-mentioned data together indicated that EGFR could response to increased IFSS.

We have demonstrated the nuclear executor function of KLF5 and biomechanical signal transducing role of MAPK signaling pathway in phenotypic switching of VSMCs mediated by increased IFSS, respectively. However, we still do not know whether EGFR activates MAPK-KLF5 signal axis. Therefore, we employed EGFR inhibitor (gefitinib) to reveal its function in the IFSS-based mechanical clue [47]. Firstly, we validated the blocking proficiency of gefitinib for EGFR in VSMCs after 3 dyn/cm² IFSS loading. The reduced *p*-EGFR and stable EGFR suggested that gefitinib could inhibit the activation of EGFR induced by increased IFSS (Figure 8G-H and S8G-H). We further investigated the potential activation of key MAPK signaling molecules, *p*-ERK and ERK, under increased IFSS conditions in the presence of gefitinib. Gefitinib treatment led to a notable reduction in *p*-ERK levels (Figure 8G and 8I), suggesting the absence of downstream MAPK pathway activation following EGFR blockade. Moreover, total KLF5 expression was markedly attenuated following gefitinib treatment (Figure 8G, 8J and 8K). Meanwhile, immunostaining of KLF5 in VSMCs with gefitinib treatment showed obvious extranuclear transportation even under IFSS stimulation (Figure 8L and 8M), which is accompanied by a substantial reduction of KLF5 in nuclear fraction (Figure 8N and 8O). These findings reinforce the pivotal role of EGFR within the mechanotransduction signaling cascade.

Subsequent investigations focused on the interplay between EGFR inhibition and VSMC phenotypic switching. As we expected, contractile markers (α -SMA and SM22 α) exhibited a significant upregulation, whereas synthetic markers (MMP2 and MMP9) were downregulated in VSMCs subjected to both increased IFSS and gefitinib exposure (Figure S8I-M). Taken together, these results imply that

IFSS-activated EGFR initiates the MAPK-KLF5 signaling axis, culminating in phenotypic switching of VSMCs.

Discussion

VSMCs play a critical role in preserving the integrity of blood vessel walls and regulating vascular

tension [49]. However, their pathological behavior, characterized by enhanced motility and proliferation, is closely linked to the development of atherosclerosis. Phenotypic switching of VSMCs, where they transition from a contractile to a synthetic phenotype, has been implicated in the initiation and progression of atherosclerosis [5].

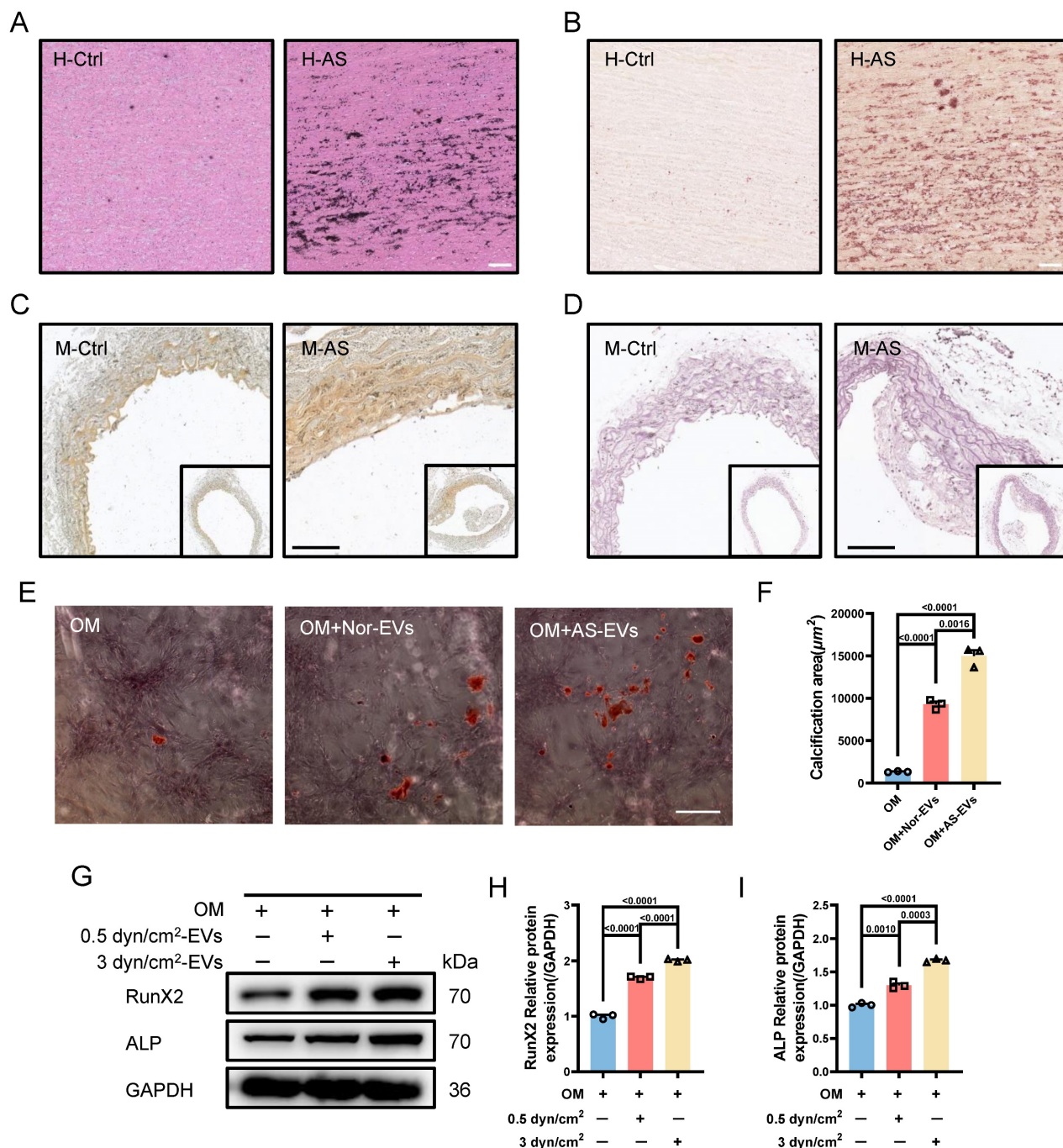


Figure 5. Synthetic VSMCs-derived EVs promote the calcification of artery. (A) Von Kossa staining shows calcium deposition in human atherosclerotic artery tissue. Scale bar, 100 μm . (B) Alizarin red S staining is performed to confirm the calcium deposition in the atherosclerotic artery tissue from human. Scale bar, 100 μm . (C, D) Von Kossa and Alizarin red S staining reveal the calcium deposition in the atherosclerotic artery tissue from mouse. Scale bar, 200 μm . (E, F) Alizarin red S staining of primary VSMCs isolated from a normal mouse artery subjected to the EVs, which is released from the primary VSMCs isolated from the atherosclerotic mouse artery. Red plaques indicate the calcification nodules. Scale bar, 20 μm . (G-I) Immunoblotting and quantitative analysis of calcification marker (RunX2, ALP) in HASMCs co-cultured with the EVs derived from HASMCs subjected to increased IFSS. OM: osteogenic induction medium. GAPDH is used as a loading control, n=3. Data are shown as mean \pm SEM. Statistical analysis was performed by one-way analysis of variance followed by the Tukey test.

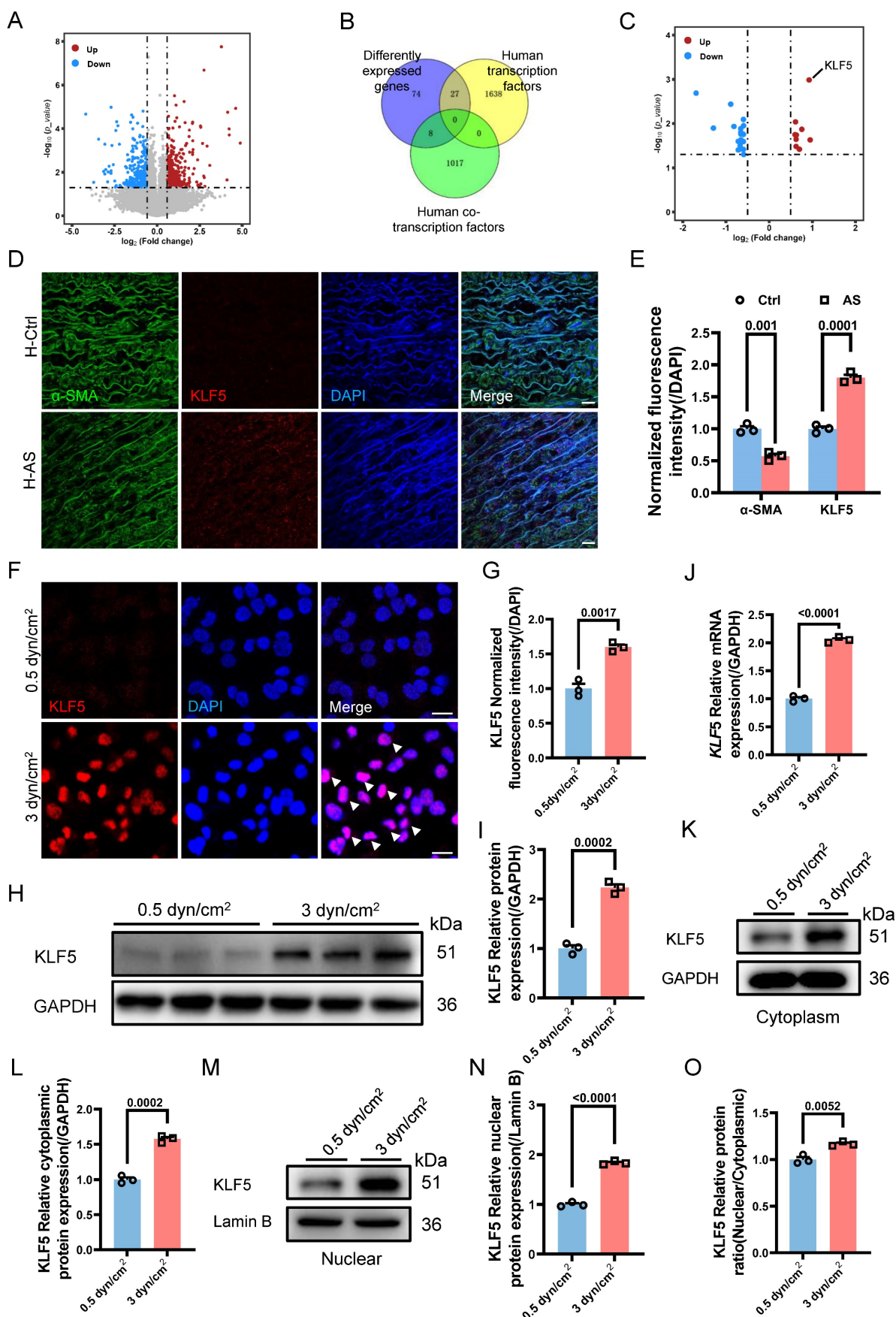


Figure 6. KLF5 drives IFSS-induced phenotypic switching of VSMCs. (A) Volcano plot of differentially expressed genes in HASMCs after subjecting to increased IFSS. Compared to the 0.5 dyn/cm² group, 393 genes were upregulated, 385 genes were downregulated, and 28,545 genes showed no significant difference in the 3 dyn/cm² group. (B) Venn analysis of the differentially expressed genes with co-transcriptional and transcriptional factors. (C) The highest expression level of KLF5 in the intersectoral genes indicated

its potential role in the VSMCs phenotypic switching. (D, E) Immunostaining and normalized fluorescence intensity analysis of KLF5 in the atherosclerotic artery from human patient. KLF5 (red), α -SMA (green), DAPI (blue). Scale bar, 20 μ m, n=3. (F, G) Immunostaining and normalized fluorescence intensity analyses of KLF5 in HASMCs subjecting to different IFSS. KLF5 (red), DAPI (blue). Scale bar, 20 μ m, n=3. (H, I) Western blot and quantitative analysis of KLF5 in HASMCs subjecting to IFSS. GAPDH is used as loading control, n=3. (J) mRNA levels of *KLF5* were analyzed by qRT-PCR. The relative abundances of transcripts were quantified and normalized to *Gapdh*, n=3. (K, L) Expression of KLF5 in the cytoplasm and quantitative analysis subjecting to IFSS. GAPDH was used as a loading control, n=3. (M, N) Expression of KLF5 in the nuclear and quantitative analysis under IFSS. Lamin B was used as a loading control, n=3. (O) The ratio of KLF5 expression in different fractions of HASMCs. Data are shown as mean \pm SEM, and statistical analysis is performed by one-way analysis of variance followed by the Tukey test.

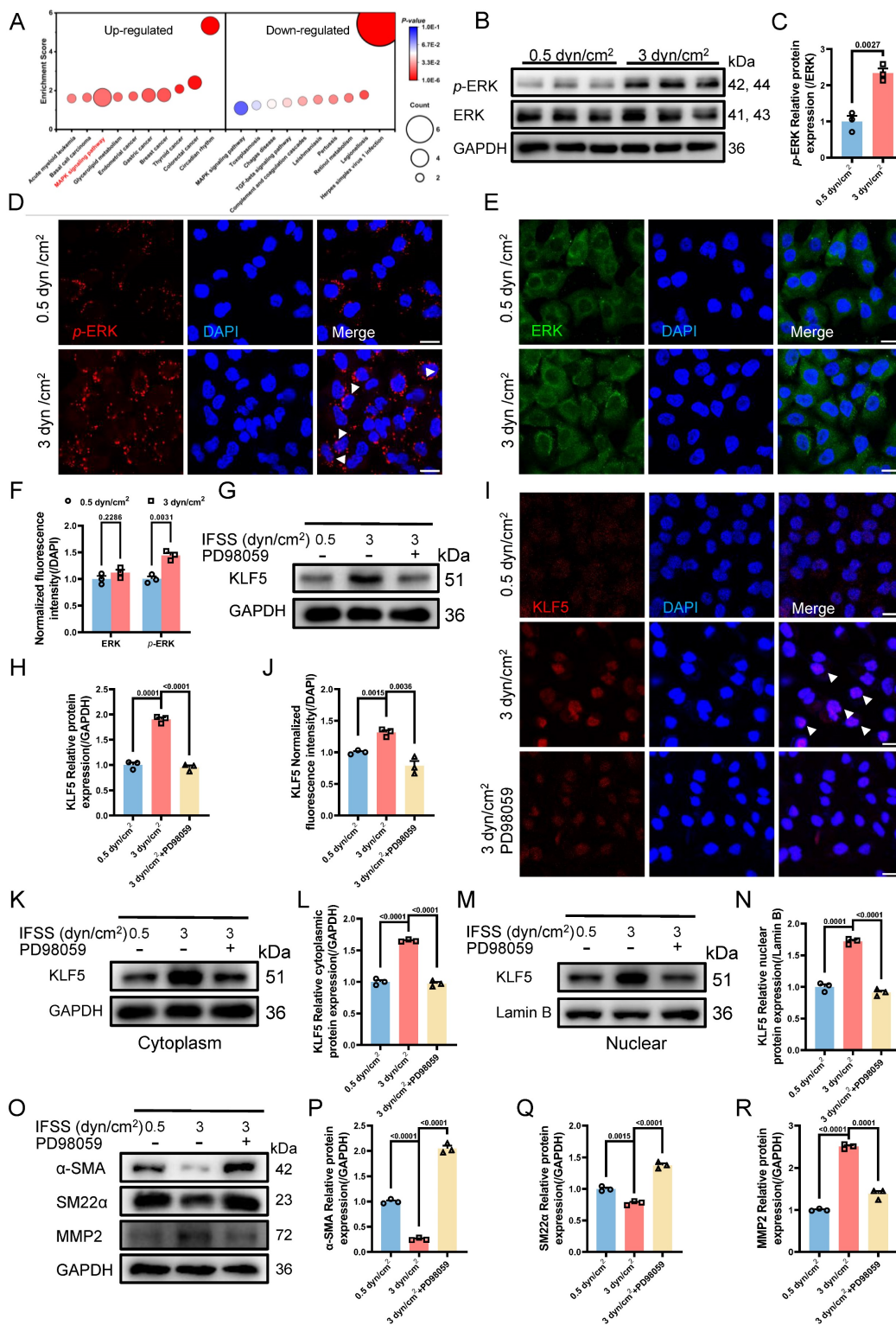


Figure 7. MAPK signaling pathway initiates KLF5 to promote VSMCs phenotypic switching. (A) RNA-seq analysis identified the MAPK signaling pathway as a candidate regulator of VSMCs phenotypic switching after 3 dyn/cm² IFSS loading. (B, C) Western blot and quantitative analysis of phosphorylated ERK (p-ERK) and ERK in HASMCs subjecting to increased IFSS. GAPDH is used as loading control, n=3. (D-F) Immunostaining and normalized fluorescence intensity analyses of p-ERK and ERK in HASMCs. White arrows signify the nuclear localization of p-ERK. p-ERK (red), ERK (green), and nuclei were counterstained with DAPI (blue). Scale bar, 20 μ m, n=3. (G, H) Western blot and quantitative analysis of KLF5 in HASMCs pre-treated with MAPK inhibitor (PD98059) upon IFSS stimulation. GAPDH is used as a loading control, n=3. (I, J) Western blot and quantitative analysis of KLF5 in HASMCs. GAPDH is used as a loading control, n=3. (K, L) Expression of KLF5 in the cytoplasm and quantitative analysis subjecting to IFSS. GAPDH was used as a loading control, n=3. (M, N) Expression of KLF5 in the nuclear and quantitative analysis under IFSS. Lamin B was used as a loading control, n=3. (O) The ratio of KLF5 expression in different fractions of HASMCs. Data are shown as mean \pm SEM, and statistical analysis is performed by one-way analysis of variance followed by the Tukey test.

Immunostaining and normalized fluorescence intensity analysis of KLF5 in HASMCs pre-treated with MAPK inhibitor (PD98059) upon IFSS stimulation. KLF5 (red), nuclei were counterstained with DAPI (blue). Scale bar, 20 μ m, n=3. **(K, L)** Expression of KLF5 in the cytoplasm and quantitative analysis pre-treated with MAPK inhibitor (PD98059) subjected to IFSS. GAPDH was used as a loading control, n=3. **(M, N)** Expression of KLF5 in the nuclear and quantitative analysis pre-treated with PD98059 under IFSS. Lamin B was used as a loading control, n=3. **(O-R)** Western blot analysis of phenotypic switching indicators (α -SMA and SM22 α , contractile marker. MMP2, synthetic marker) in HASMCs pre-treated with MAPK inhibitor (PD98059) and quantitative analysis of phenotypic switching indicators upon IFSS stimulation. GAPDH is used as a loading control, n=3. Unpaired t-tests were used to compare variables with normal distribution and homogeneity of variance. All data are presented as mean \pm SEM.

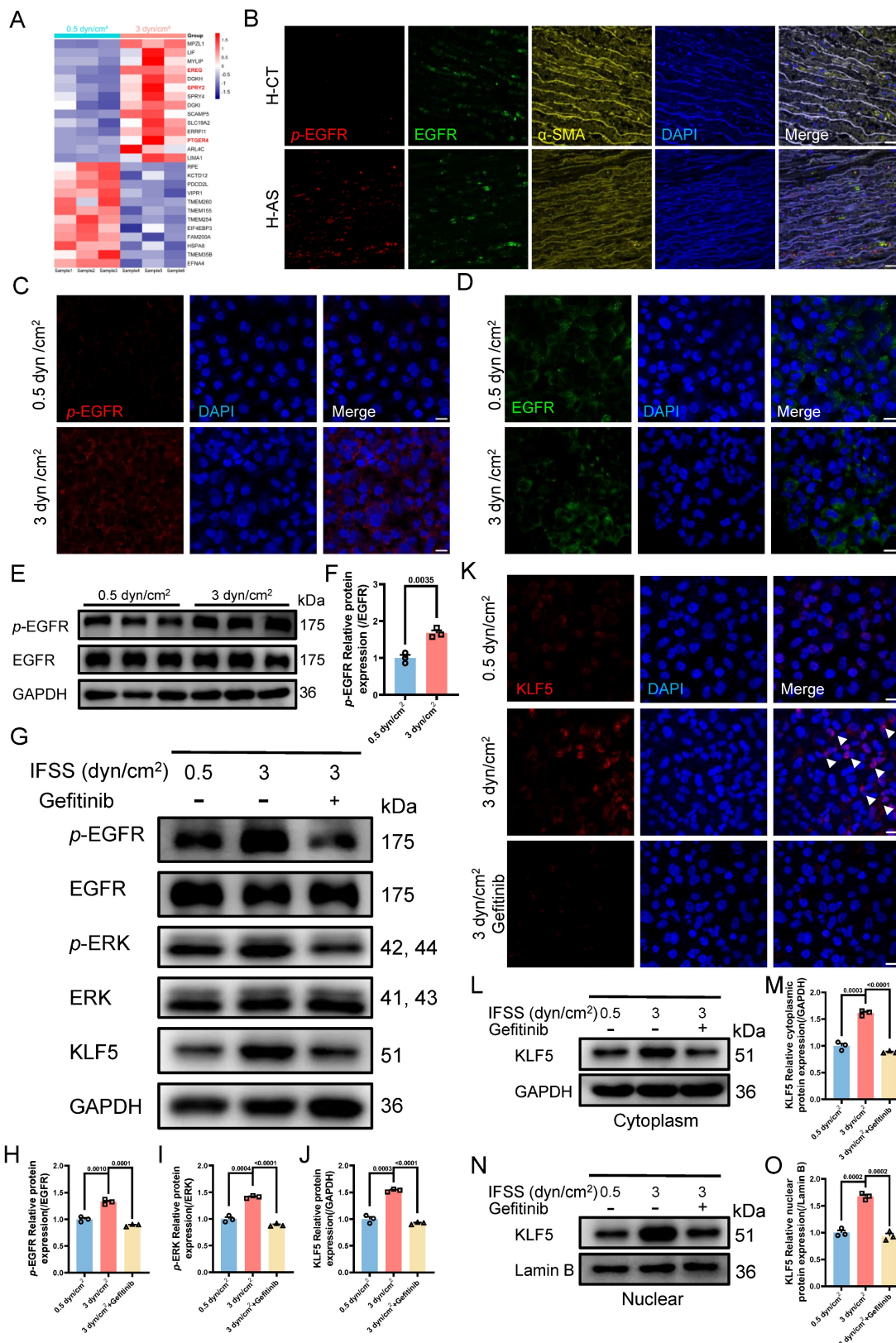


Figure 8. The IFSS-based mechanical clue is initiated by EGFR. **(A)** Heatmap illustrates the changes in membrane-bound genes after increased IFSS exposure. 14 genes show a significant increase after 3 dyn/cm² IFSS loading. Three genes highlighted in red are associated with the EGFR receptor. **(B)** Immunostaining shows the location and

expression of p-EGFR (red), EGFR (green) and VSMCs phenotype (α -SMA, yellow) in human atherosclerotic arteries. Cell nuclei were counterstained with DAPI (blue). The red channel was linearly enhanced by 20% for clear view. Scale bar, 20 μ m, n=3. (C, D) Immunostaining of p-EGFR and EGFR in HASMCs. p-EGFR (red), EGFR (green), and nuclei were counterstained with DAPI (blue). Scale bar, 20 μ m, n=3. (E, F) Western blot and quantitative analysis of phosphorylated EGFR (p-EGFR) and EGFR in HASMCs with elevated IFSS. GAPDH is used as loading control, n=3. (G-J) Western blot and quantitative analysis of p-EGFR, EGFR, p-ERK, ERK and KLF5 in HASMCs with pre-treatment of EGFR inhibitor (gefitinib) followed by IFSS stimulation. GAPDH is used as a loading control, n=3. (K) Immunostaining of KLF5 in HASMCs pre-treated with EGFR inhibitor (gefitinib) upon IFSS stimulation. KLF5 (red), nuclei were counterstained with DAPI (blue). Scale bar, 20 μ m, n=3. (L, M) Expression of KLF5 in the cytoplasm and quantitative analysis in HASMCs pre-treated with gefitinib subjected to IFSS. GAPDH was used as a loading control, n=3. (N, O) KLF5 expression in nuclear and quantitative analysis in HASMCs pre-treated with gefitinib under IFSS. Lamin B was used as a loading control, n=3. Unpaired t-tests were used to compare variables with normal distribution and homogeneity of variance. All data are presented as mean \pm SEM.

After phenotypic switching, VSMCs lose the contractile phenotype marker gene, including smooth muscle cell myosin heavy chain (MYH11), 22-kDa SMC lineage-restricted protein (SM22 α /tagln), and express synthetic marker genes, such as *MMP2/9*. Upon phenotypic switching, VSMCs activate inflammatory pathways, leading to increased macrophage recruitment and the advancement of atherosclerosis [50]. Therefore, understanding VSMCs phenotypic switching has been recognized as a fundamental aspect in atherosclerosis research. More importantly, investigating the regulatory factors and molecular mechanisms driving phenotypic switching is necessary for developing therapeutic strategies targeting VSMCs. However, the lack of clarity regarding the regulatory factors and underlying molecular mechanisms has hindered the development of direct interventional therapies to prevent phenotypic switching in VSMCs.

Various stimuli, such as endothelial injury, pro-inflammatory cytokines, oxidative stress, extracellular matrix (ECM), and mechanical force, have been identified as triggers for phenotypic switching in VSMCs [51, 52]. Among these stimuli, biomechanical factors have gained significant attention due to their direct regulatory role and their potential contribution to major arterial diseases through mechanobiological instabilities [10, 53, 54]. Specifically, IFSS plays a pivotal role in regulating various biological behaviors of VSMCs and has been associated with major arterial diseases [10, 12, 13]. However, accurately determining the precise value of IFSS experienced by VSMCs in atherosclerotic arteries has been challenging. Fortunately, the rapid progress in computational fluid dynamic simulations enabled us to estimate the *in vivo* IFSS realistically [55]. To address this issue, we employed computational fluid dynamic simulations and incorporated patient data to estimate IFSS values with greater accuracy. To our knowledge, this is the first time that the precise value of IFSS in atherosclerotic artery was calculated based on the parameters from human artery samples. Subsequently, we conducted *in vitro* experiments to validate the promoting role of IFSS from our numerical calculation in regulating VSMCs phenotypic switching. After subjecting to the calculated atherosclerotic IFSS, phenotypic switching of VSMCs was observed, which is consistent with the synthetic

VSMCs in human atherosclerotic arteries. Our study successfully confirmed the role of increased IFSS in promoting VSMCs phenotypic switching, emphasizing its significance in the context of atherosclerosis. Therefore, increased IFSS plays a decisive role in the occurrence and progression of VSMCs phenotypic switching and holds potential as a diagnostic indicator for atherosclerosis. On the other hand, extensive research has been conducted on IFSS in many diseases, including cancer and Alzheimer's disease, utilizing it as a quantitative physical parameter for disease investigation, clinical diagnosis, and treatment [56, 57]. Thus, these findings highlight the potential of IFSS as a diagnostic indicator for atherosclerosis. However, studying interstitial flow presents significant challenges, necessitating the development of innovative approaches to effectively capture and assess its variations.

In addition to phenotypic switching, the secretion of EVs derived from VSMCs significantly elevated after exposure to increased IFSS. These EVs played a role in promoting VSMCs calcification, representing another form of phenotypic switching. Although cargos of the pro-calcified EVs is not explored in this study, it has been shown that sphingolipid phosphodiesterase 3, phosphatidylserine, annexin A6, and microRNAs (e.g. miR143, miR221, and miR222) contained in EVs are the potential mediator for other cells calcification [58-60]. Previous studies have shown that externally added VSMC-derived EVs induce phenotypic switching under oxidative stress [20]. Therefore, we wondered whether the synthetic VSMCs secreted more EVs or whether the EVs accelerated the phenotypic switching of VSMCs in the atherosclerotic artery. Co-culturing VSMCs with EVs derived from synthetic VSMCs did not induce phenotypic switching in neighboring contractile VSMCs. Our investigation revealed that phenotypic switching with increased IFSS stimulation acts as an upstream regulator of pro-calcified EVs secretion. Besides, other research indicated that the mechanism underlying the observed correlations between mechanical stress and EV biogenesis is complex and depends significantly on both the parent cell type and the nature of the applied stress [61]. Therefore, the relationship between shear stress and the release of EVs remains a focal point for future research in cardiovascular diseases [62].

The molecular mechanisms underlying increased IFSS-induced phenotypic switching of VSMCs are not fully understood. Various signaling pathways, including DNA methylation/TET methylcytosine dioxygenase 2, Hippo-YAP signaling pathway, Notch signaling pathway, and integrin β 3-mediated signaling cascades, have been implicated in regulating VSMC phenotypic switching [63]. However, whether these pathways respond to IFSS is not known. Here, we clarified that MAPK signaling pathway is activated by increased IFSS in VSMCs through conducting RNA-sequence and pharmaceutical inhibition. Next, we sought to unravel the executor responding to the biomechanical clue passed by MAPK signaling pathway. Krüppel-like factors (KLFs) are a group of DNA-binding transcription factors involved in the development, metabolism and other cellular mechanisms [64]. Unlike the well-known KLF4, the mechanobiological role of KLF5 in IFSS-induced phenotypic switching of VSMCs remains unclear [44, 65-68]. Our experimental findings revealed that KLF5 mediates phenotypic switching under increased IFSS conditions. The upregulation of total and nuclear KLF5 in VSMCs exposed to increased IFSS suggests its transcriptional regulatory function on synthetic phenotype genes. As a basic transcriptional factor, KLF5 is well known to regulate target gene transcription [69]. The expression and activation of KLF5 are regulated by various signaling pathways and post-translational modification. The signaling pathways that regulate KLF5 expression have mostly been explored, with evidence showing that FOXO1 and YAP promoted KLF5 expression in cardiomyocytes and renal tubular cells respectively via direct binding on the KLF5 promoter [70, 71]. The phosphorylated KLF5 on the different sites (such as S153 and S303) promotes the transactivating function of KLF5. In contrast, SUMOylation on K162 and K209 by enzyme SUMO1 converts KLF5 from a transcription activator to an inhibitor. On the other hand, activation of KLF5 could initiate some signaling pathway. For example, the loss of KLF5 acetylation at K358 in basal progenitors promotes luminal commitment by activating Notch signaling [72]. Additionally, KLF5 is identified as the responsive gene to activating Wnt signaling pathway [73]. Regarding therapeutic potential, KLF5 inhibition has been proposed as a strategy for treating atherosclerosis. Preclinical studies showed that systemic pharmacological KLF5 inhibition protects against heart disease, although prolonged inhibition may lead to cardiomyopathy [44]. Therefore, understanding the spatial and temporal expression profile of KLF5 during disease progression is necessary to identify the optimal timing and extent of

an inhibitory intervention.

EGFR has been identified as a mechanosensitive molecule, when subjected to compressive forces on airway epithelial cells, initiates an EGFR-dependent mechanotransduction pathway, culminating in enhanced phosphorylation of downstream kinases [74]. In ovarian cancer cells, abnormal hemodynamics can consistently elevate EGFR expression and activity, primarily through decreased receptor degradation and increased recycling, which promotes cell proliferation, survival, and chemoresistance [75, 76]. These findings highlight the pivotal role of EGFR in mechanotransduction processes. Additionally, post-translational modification contributes to the activation of EGFR upon biomechanical stimuli. For example, methylation of EGFR at Arg 1175 by PRMT5 enhances its phosphorylation at Tyr 1173, and critically influences ERK activity within the EGFR signaling pathway [77]. The intricate balance between methylation and phosphorylation of EGFR finely regulates various cellular processes response to mechanical stimuli. Our results suggest that IFSS stimulation significantly upregulated the expression of *p*-EGFR in VSMCs. Furthermore, after inhibiting EGFR activation in VSMCs upon increased IFSS, the downstream factor *p*-ERK was markedly decreased. Collectively, we further validated the crucial role of EGFR in converting the biomechanical stimulus into a biochemical signal that activates the downstream MAPK signaling pathway.

Through the global gene expression profile and pharmacological inhibition, we confirmed that the MAPK-ERK signaling pathway acts as the upstream regulator of KLF5 in the transduction of flow-based mechanical cues. Pharmacological inhibition of ERK impedes the increased IFSS-induced nuclear accumulation of KLF5 and suppresses its expression. These findings align with previous studies showing the activating MAPK signaling pathway in VSMCs after sphingosine 1-phosphate (S1P) stimulation, which also results in an elevated expression of KLF5 [78]. Blocking MAPK-ERK signaling has been proposed as an alternative therapy for inhibiting KLF5. Emerging technologies, such as PROteolysis TARgeting Chimeras (PROTACs) have attracted great attention for finding another approach to overcome the drug resistance caused by small molecular drugs [79]. The Heightman group designed representative PROTACs of ERK1 and ERK2. After 16 h post-ERK-CLIPTAC was added to the cell, the degradation of ERK1 or ERK2 was observed [80]. However, the therapeutic effect of this ERK-CLIPTAC was not investigated in atherosclerotic tissue or cells.

In conclusion, our study provides insights into the mechanobiological role of EGFR-MAPK-KLF5

signaling axis in IFSS-induced phenotypic switching of VSMCs, which is implicated in the development of atherosclerosis, targeting KLF5 or its upstream regulator EGFR and MAPK signaling pathway through small molecular drugs or emerging technologies, such as PROTACs holds promise as a therapeutic approach to prevent VSMCs phenotypic switching and ameliorate atherosclerosis. These findings contribute to our understanding of the underlying mechanisms in the progression of atherosclerosis and offer potential avenues for precision medicine and personalized treatment.

The current study is constrained by the limited availability of healthy artery tissue from normal human donors, mainly stemming from the limited availability of heart transplant surgeries. Therefore, some parameters such as thickness and porosity, essential for representing various layers of a healthy artery, are lacking, potentially leading to deviations in the calculation of IFSS. Future research should focus on increasing the sample size of healthy artery tissue and ideally integrating pathological grading into the calculation process to explore the mechanistic aspects further, while recognizing that observing enhanced IFSS in the atherosclerotic artery is still plausible. Furthermore, while we successfully verified the involvement of the KLF5 gene in the cell IFSS loading model through genetic blocking, its role *in vivo* remains to be validated. Prior studies have indicated that systemic and conditional KLF5 gene deletions lead to embryonic lethality, presenting a challenge for *in vivo* experiments [81, 82]. To overcome this hurdle, we propose employing adeno-associated virus (AAV) in combination with CRISPR/Cas9, which offers a promising solution due to its post-birth gene editing capabilities. Moreover, our study has effectively demonstrated that IFSS activates the transcriptional function of KLF5. Nevertheless, a deeper investigation is still warranted to understand how the activated KLF5 regulates the release of pro-calcified EVs to acquire comprehensive insights into the underlying mechanisms involved.

Abbreviations

ALP: alkaline phosphatase; ApoE: apolipoprotein E-deficient; AS: atherosclerosis; α -SMA: alpha smooth muscle actin; CD31: cluster of differentiation 31; CD63: cluster of differentiation 63; CVD: cardiovascular diseases; EGFR: epidermal growth factor receptor; ERK: extracellular signal-regulated kinases; EVs: extracellular vesicles; FOXO1: forkhead box o1; IFSS: interstitial fluid shear stress; KLF4: krüppel-like factor 4; KLF5: krüppel-like factor 5; MAPK: mitogen-activated protein kinases; MMP2: matrix metalloproteinase 2; MMP9: matrix

metalloproteinase 2; MYH11: myosin heavy chain 11; p-ERK: phosphorylated extracellular signal-regulated kinases; PROTACs: proteolysis targeting chimera; Runx2: runt-related transcription factor 2; TF: transcription factor; TSG101: tumor susceptibility gene 101; VSMCs: vascular smooth muscle cells; WSS: wall shear stress.

Supplementary Material

Supplementary materials and methods, figures and tables. <https://www.ijbs.com/v20p2727s1.pdf>

Acknowledgments

The authors thank Hui Wang from Pub-Lab Platform, West China School of Basic Medical Sciences and Forensic Medicine, Sichuan University for assistance with the testing process.

Funding

This study was supported by the National Natural Science Foundation of China (11932014, 12372315, 32371369), Sichuan Science and Technology Program (2022NSFSC0765, 2022ZYD0079), Science and Technology Innovation Project of JinFeng Laboratory, Chongqing, China (jfkjyf202203001).

Ethics approval and consent to participate

The animal study was conducted in accordance with the guidelines set by the China Council on Animal Care and was approved by the Medical Ethics Committee of Sichuan University.

Competing Interests

The authors have declared that no competing interest exists.

References

- Libby P, Buring JE, Badimon L, Hansson GK, Deanfield J, Bittencourt MS, et al. Atherosclerosis. *Nat Rev Dis Primers*. 2019; 5: 56.
- Soehnlein O, Libby P. Targeting inflammation in atherosclerosis - from experimental insights to the clinic. *Nat Rev Drug Discov*. 2021; 20: 589-610.
- Libby P. The changing landscape of atherosclerosis. *Nature*. 2021; 592: 524-33.
- Liu M, Gomez D. Smooth Muscle Cell Phenotypic Diversity. *Arterioscler Thromb Vasc Biol*. 2019; 39: 1715-23.
- Bennett MR, Sinha S, Owens GK. Vascular Smooth Muscle Cells in Atherosclerosis. *Circ Res*. 2016; 118: 692-702.
- Gomez D, Owens GK. Smooth muscle cell phenotypic switching in atherosclerosis. *Cardiovasc Res*. 2012; 95: 156-64.
- Libby P, Everett BM. Novel Antiatherosclerotic Therapies. *Arterioscler Thromb Vasc Biol*. 2019; 39: 538-45.
- Miyazaki Y, Suwannasom P, Sotomi Y, Abdelghani M, Tummala K, Katagiri Y, et al. Single or dual antiplatelet therapy after PCI. *Nat Rev Cardiol*. 2017; 14: 294-303.
- Jukema JW, Verschuren JJ, Ahmed TA, Quax PH. Restenosis after PCI. Part 1: pathophysiology and risk factors. *Nat Rev Cardiol*. 2011; 9: 53-62.
- Humphrey JD, Schwartz MA. Vascular Mechanobiology: Homeostasis, Adaptation, and Disease. *Annu Rev Biomed Eng*. 2021; 23: 1-27.
- Takeda H, Komori K, Nishikimi N, Nimura Y, Sokabe M, Naruse K. Bi-phasic activation of eNOS in response to uni-axial cyclic stretch is mediated by differential mechanisms in BAECs. *Life Sci*. 2006; 79: 233-9.
- Shi ZD, Tarbell JM. Fluid flow mechanotransduction in vascular smooth muscle cells and fibroblasts. *Ann Biomed Eng*. 2011; 39: 1608-19.
- Kang H, Liu J, Sun A, Liu X, Fan Y, Deng X. Vascular smooth muscle cell glycocalyx mediates shear stress-induced contractile responses via a Rho

- kinase (ROCK)-myosin light chain phosphatase (MLCP) pathway. *Sci Rep.* 2017; 7: 42092.
14. Civelek M, Ainslie K, Garanich JS, Tarbell JM. Smooth muscle cells contract in response to fluid flow via a Ca²⁺-independent signaling mechanism. *J Appl Physiol* (1985). 2002; 93: 1907-17.
 15. Jia X, Yang J, Song W, Li P, Wang X, Guan C, et al. Involvement of large conductance Ca²⁺-activated K⁺ channel in laminar shear stress-induced inhibition of vascular smooth muscle cell proliferation. *Pflugers Arch.* 2013; 465: 221-32.
 16. Proudfoot D, Skepper JN, Hegyi L, Bennett MR, Shanahan CM, Weissberg PL. Apoptosis regulates human vascular calcification in vitro: evidence for initiation of vascular calcification by apoptotic bodies. *Circ Res.* 2000; 87: 1055-62.
 17. Shanahan CM. Mechanisms of vascular calcification in CKD-evidence for premature ageing? *Nat Rev Nephrol.* 2013; 9: 661-70.
 18. Tyson KL, Reynolds JL, McNair R, Zhang Q, Weissberg PL, Shanahan CM. Osteo/chondrocytic transcription factors and their target genes exhibit distinct patterns of expression in human arterial calcification. *Arterioscler Thromb Vasc Biol.* 2003; 23: 489-94.
 19. Cheng L, Hill AF. Therapeutically harnessing extracellular vesicles. *Nat Rev Drug Discov.* 2022; 21: 379-99.
 20. Furmanik M, Chatrou M, van Gorp R, Akbulut A, Willems B, Schmidt H, et al. Reactive Oxygen-Forming Nox5 Links Vascular Smooth Muscle Cell Phenotypic Switching and Extracellular Vesicle-Mediated Vascular Calcification. *Circ Res.* 2020; 127: 911-27.
 21. Vajen T, Benedikter BJ, Heinzmann ACA, Vasina EM, Henskens Y, Parsons M, et al. Platelet extracellular vesicles induce a pro-inflammatory smooth muscle cell phenotype. *J Extracell Vesicles.* 2017; 6: 1322454.
 22. Jia LX, Zhang WM, Li TT, Liu Y, Piao CM, Ma YC, et al. ER stress dependent microparticles derived from smooth muscle cells promote endothelial dysfunction during thoracic aortic aneurysm and dissection. *Clin Sci (Lond).* 2017; 131: 1287-99.
 23. Akerman AW, Blanding WM, Stroud RE, Nadeau EK, Mukherjee R, Ruddy JM, et al. Elevated Wall Tension Leads to Reduced miR-133a in the Thoracic Aorta by Exosome Release. *J Am Heart Assoc.* 2019; 8: e010332.
 24. Yu H, Hou Z, Xiang M, Yang F, Ma J, Yang L, et al. Arsenic trioxide activates yes-associated protein by lysophosphatidic acid metabolism to selectively induce apoptosis of vascular smooth muscle cells. *Biochim Biophys Acta Mol Cell Res.* 2022; 1869: 119211.
 25. Hickson SS, Butlin M, Graves M, Taviani V, Avolio AP, McEniery CM, et al. The relationship of age with regional aortic stiffness and diameter. *JACC-Cardiovasc Imag.* 2010; 3: 1247-55.
 26. Zhang MH. *Engineering Fluid Mechanics.* Machinery Industry Press; 2018.
 27. Yao W, Li Y, Ding G. Interstitial fluid flow: the mechanical environment of cells and foundation of meridians. *Evid Based Complement Alternat Med.* 2012; 2012: 853516.
 28. Rutkowski JM, Swartz MA. A driving force for change: interstitial flow as a morphoregulator. *Trends Cell Biol.* 2007; 17: 44-50.
 29. Gonzales AL, Garcia ZI, Amberg GC, Earley S. Pharmacological inhibition of TRPM4 hyperpolarizes vascular smooth muscle. *Am J Physiol Cell Physiol.* 2010; 299: C1195-202.
 30. Hu NW, Rodriguez CD, Rey JA, Rozenblum MJ, Courtney CP, Balogh P, et al. Estimation of shear stress values along endothelial tip cells past the lumen of capillary sprouts. *Microvasc Res.* 2022; 142.
 31. Yu H, He J, Su G, Wang Y, Fang F, Yang W, et al. Fluid shear stress activates YAP to promote epithelial-mesenchymal transition in hepatocellular carcinoma. *Mol Oncol.* 2021; 15: 3164-83.
 32. Barallobre-Barreiro J, Loeys B, Mayr M, Rienks M, Verstraeten A, Kovacic JC. Extracellular Matrix in Vascular Disease, Part 2/4: JACC Focus Seminar. *J Am Coll Cardiol.* 2020; 75: 2189-203.
 33. Boulanger CM, Loyer X, Rautou PE, Amabile N. Extracellular vesicles in coronary artery disease. *Nat Rev Cardiol.* 2017; 14: 259-72.
 34. Yang N, Vafai K. Modeling of low-density lipoprotein (LDL) transport in the artery – effects of hypertension. *Int J Heat Mass Tran.* 2006; 49: 850-67.
 35. Shi ZD, Ji XY, Qazi H, Tarbell JM. Interstitial flow promotes vascular fibroblast, myofibroblast, and smooth muscle cell motility in 3-D collagen I via upregulation of MMP-1. *Am J Physiol Heart Circ Physiol.* 2009; 297: H1225-34.
 36. Shou Y, Jan KM, Rumschitzki DS. Transport in rat vessel walls. I. Hydraulic conductivities of the aorta, pulmonary artery, and inferior vena cava with intact and denuded endothelia. *Am J Physiol Heart Circ Physiol.* 2006; 291: H2758-71.
 37. Jain M, Dev R, Doddapattar P, Kon S, Dhanesha N, Chauhan AK. Integrin alpha9 regulates smooth muscle cell phenotype switching and vascular remodeling. *JCI Insight.* 2021; 6.
 38. Menaceur C, Dusailly O, Gosselet F, Fenart L, Saint-Pol J. Vesicular Trafficking, a Mechanism Controlled by Cascade Activation of Rab Proteins: Focus on Rab27. *Biology (Basel).* 2023; 12.
 39. Ostrowski M, Carmo NB, Krumeich S, Fanget I, Raposo G, Savina A, et al. Rab27a and Rab27b control different steps of the exosome secretion pathway. *Nat Cell Biol.* 2010; 12: 19-30; sup pp 1-13.
 40. Llorente-Cortes V, Otero-Vinas M, Camino-Lopez S, Llampayas O, Badimon L. Aggregated low-density lipoprotein uptake induces membrane tissue factor procoagulant activity and microparticle release in human vascular smooth muscle cells. *Circulation.* 2004; 110: 452-9.
 41. Brousseau C, Morissette G, Fortin JP, Marceau F, Petitclerc E. Tumor cells expressing tissue factor influence the migration of smooth muscle cells in a catalytic activity-dependent way. *Can J Physiol Pharmacol.* 2009; 87: 694-701.
 42. Otsuka F, Sakakura K, Yahagi K, Joner M, Virmani R. Has our understanding of calcification in human coronary atherosclerosis progressed? *Arterioscler Thromb Vasc Biol.* 2014; 34: 724-36.
 43. Lambert SA, Jolma A, Campitelli LF, Das PK, Yin Y, Albu M, et al. The Human Transcription Factors. *Cell.* 2018; 172: 650-65.
 44. Palioura D, Lazou A, Drosatos K. Kruppel-like factor (KLF)5: An emerging foe of cardiovascular health. *J Mol Cell Cardiol.* 2022; 163: 56-66.
 45. Lavoie H, Gagnon J, Therrien M. ERK signalling: a master regulator of cell behaviour, life and fate. *Nat Rev Mol Cell Biol.* 2020; 21: 607-32.
 46. Schwartz AD, Hall CL, Barney LE, Babbitt CC, Peyton SR. Integrin alpha(6) and EGFR signaling converge at mechanosensitive calpain 2. *Biomaterials.* 2018; 178: 73-82.
 47. Rubsam M, Mertz AF, Kubo A, Marg S, Jungst C, Goranci-Buzhala G, et al. E-cadherin integrates mechanotransduction and EGFR signaling to control junctional tissue polarization and tight junction positioning. *Nat Commun.* 2017; 8: 1250.
 48. Liu Q, Yu S, Zhao W, Qin S, Chu Q, Wu K. EGFR-TKIs resistance via EGFR-independent signaling pathways. *Mol Cancer.* 2018; 17: 53.
 49. Lacollet P, Regnault V, Laurent S. Mechanisms of Arterial Stiffening: From Mechanotransduction to Epigenetics. *Arterioscler Thromb Vasc Biol.* 2020; 40: 1055-62.
 50. Ackers-Johnson M, Talasila A, Sage AP, Long X, Bot I, Morrell NW, et al. Myocardin regulates vascular smooth muscle cell inflammatory activation and disease. *Arterioscler Thromb Vasc Biol.* 2015; 35: 817-28.
 51. Zhang MJ, Zhou Y, Chen L, Wang YQ, Wang X, Pi Y, et al. An overview of potential molecular mechanisms involved in VSMC phenotypic modulation. *Histochem Cell Biol.* 2016; 145: 119-30.
 52. Owens GK, Kumar MS, Wamhoff BR. Molecular regulation of vascular smooth muscle cell differentiation in development and disease. *Physiol Rev.* 2004; 84: 767-801.
 53. Baeyens N, Schwartz MA. Biomechanics of vascular mechanosensation and remodeling. *Mol Biol Cell.* 2016; 27: 7-11.
 54. Tarbell JM, Shi ZD, Dunn J, Jo H. Fluid Mechanics, Arterial Disease, and Gene Expression. *Annu Rev Fluid Mech.* 2014; 46: 591-614.
 55. Galie PA, Nguyen DH, Choi CK, Cohen DM, Janney PA, Chen CS. Fluid shear stress threshold regulates angiogenic sprouting. *Proc Natl Acad Sci Usa.* 2014; 111: 7968-73.
 56. Liu WT, Cao YP, Zhou XH, Han D. Interstitial Fluid Behavior and Diseases. *Adv Sci (Weinh).* 2022; 9: e2100617.
 57. Polacheck WJ, Charest JL, Kamm RD. Interstitial flow influences direction of tumor cell migration through competing mechanisms. *P Natl Acad Sci Usa.* 2011; 108: 11115-20.
 58. Yang J, Pei T, Su GY, Duan PY, Liu XH. AnnexinA6: a potential therapeutic target gene for extracellular matrix mineralization. *Front Cell Dev Biol.* 2023; 11.
 59. Kapustin AN, Shanahan CM. Emerging roles for vascular smooth muscle cell exosomes in calcification and coagulation. *J Physiol-London.* 2016; 594: 2905-14.
 60. Li TT, Yu HC, Zhang DM, Feng T, Miao MC, Li JW, et al. Matrix Vesicles as a Therapeutic Target for Vascular Calcification. *Front Cell Dev Biol.* 2022; 10.
 61. Thompson W, Papoutsakis ET. The role of biomechanical stress in extracellular vesicle formation, composition and activity. *Biotechnol Adv.* 2023; 66: 108158.
 62. Jin Y, Ma L, Zhang W, Yang W, Feng Q, Wang H. Extracellular signals regulate the biogenesis of extracellular vesicles. *Biol Res.* 2022; 55: 35.
 63. Chakraborty R, Chatterjee P, Dave JM, Ostriker AC, Greif DM, Rzuclidlo EM, et al. Targeting smooth muscle cell phenotypic switching in vascular disease. *JVS Vasc Sci.* 2021; 2: 79-94.
 64. McConnell BB, Yang VW. Mammalian Kruppel-like factors in health and diseases. *Physiol Rev.* 2010; 90: 1337-81.
 65. Hoshino Y, Kurabayashi M, Kanda T, Hasegawa A, Sakamoto H, Okamoto E, et al. Regulated expression of the BTE2 transcription factor in vascular smooth muscle cells: analysis of developmental and pathological expression profiles shows implications as a predictive factor for restenosis. *Circulation.* 2000; 102: 2528-34.
 66. Li Y, Xiong Z, Yan W, Gao E, Cheng H, Wu G, et al. Branched chain amino acids exacerbate myocardial ischemia/reperfusion vulnerability via enhancing GCN2/ATF6/PPAR-alpha pathway-dependent fatty acid oxidation. *Theranostics.* 2020; 10: 5623-40.
 67. Kawai-Kowase K, Kurabayashi M, Hoshino Y, Ohyama Y, Nagai R. Transcriptional activation of the zinc finger transcription factor BTE2 gene by Egr-1 through mitogen-activated protein kinase pathways in vascular smooth muscle cells. *Circ Res.* 1999; 85: 787-95.
 68. Shankman LS, Gomez D, Cherepanova OA, Salmon M, Alencar GF, Haskins RM, et al. KLF4-dependent phenotypic modulation of smooth muscle cells has a key role in atherosclerotic plaque pathogenesis. *Nat Med.* 2016; 22: 217-.
 69. Dong JT, Chen C. Essential role of KLF5 transcription factor in cell proliferation and differentiation and its implications for human diseases. *Cell Mol Life Sci.* 2009; 66: 2691-706.
 70. Kyriazis ID, Hoffman M, Gaignebet L, Lucchese AM, Markopoulou E, Palioura D, et al. KLF5 Is Induced by FOXO1 and Causes Oxidative Stress and Diabetic Cardiomyopathy. *Circ Res.* 2021; 128: 335-57.

71. Liu Y, Wang Y, Xu C, Zhang Y, Wang Y, Qin J, et al. Activation of the YAP/KLF5 transcriptional cascade in renal tubular cells aggravates kidney injury. *Mol Ther.* 2024.
72. Zhang BT, Xia SY, Liu MC, Li XW, Shuai SM, Tao W, et al. Interruption of Klf5 acetylation in basal progenitor cells promotes luminal commitment by activating Notch signaling. *J Genet Genomics.* 2022; 49: 579-82.
73. Taneyhill L, Pennica D. Identification of Wnt responsive genes using a murine mammary epithelial cell line model system. *BMC Dev Biol.* 2004; 4: 6.
74. Shiomi T, Tschumperlin DJ, Park JA, Sunnarborg SW, Horiuchi K, Blobel CP, et al. TNF- α -converting enzyme/a disintegrin and metalloprotease-17 mediates mechanotransduction in murine tracheal epithelial cells. *Am J Respir Cell Mol Biol.* 2011; 45: 376-85.
75. Rizvi I, Gurkan UA, Tasoglu S, Alagic N, Celli JP, Mensah LB, et al. Flow induces epithelial-mesenchymal transition, cellular heterogeneity and biomarker modulation in 3D ovarian cancer nodules. *Proc Natl Acad Sci Usa.* 2013; 110: E1974-E83.
76. Luo Y, Tang H, Zhang Z, Zhao R, Wang C, Hou W, et al. Pharmacological inhibition of epidermal growth factor receptor attenuates intracranial aneurysm formation by modulating the phenotype of vascular smooth muscle cells. *CNS Neurosci Ther.* 2022; 28: 64-76.
77. Hsu JM, Chen CT, Chou CK, Kuo HP, Li LY, Lin CY, et al. Crosstalk between Arg 1175 methylation and Tyr 1173 phosphorylation negatively modulates EGFR-mediated ERK activation. *Nat Cell Biol.* 2011; 13: 174-U51.
78. Usui S, Sugimoto N, Takuwa N, Sakagami S, Takata S, Kaneko S, et al. Blood lipid mediator sphingosine 1-phosphate potently stimulates platelet-derived growth factor-A and -B chain expression through SIP1-Gi-Ras-MAPK-dependent induction of Kruppel-like factor 5. *J Biol Chem.* 2004; 279: 12300-11.
79. He M, Cao C, Ni Z, Liu Y, Song P, Hao S, et al. PROTACs: great opportunities for academia and industry (an update from 2020 to 2021). *Signal Transduct Target Ther.* 2022; 7: 181.
80. Lebraud H, Wright DJ, Johnson CN, Heightman TD. Protein Degradation by In-Cell Self-Assembly of Proteolysis Targeting Chimeras. *ACS Cent Sci.* 2016; 2: 927-34.
81. Ema M, Mori D, Niwa H, Hasegawa Y, Yamanaka Y, Hitoshi S, et al. Kruppel-like factor 5 is essential for blastocyst development and the normal self-renewal of mouse ESCs. *Cell Stem Cell.* 2008; 3: 555-67.
82. Lin SC, Wani MA, Whitsett JA, Wells JM. Klf5 regulates lineage formation in the pre-implantation mouse embryo. *Development.* 2010; 137: 3953-63.